MONTE CARLO STUDY OF SUPERNOVA NEUTRINO SPECTRA FORMATION

Mathias Th. Keil and Georg G. Raffelt
Max-Planck-Institut für Physik (Werner-Heisenberg-Institut)
Föhringer Ring 6, 80805 München, Germany

Hans-Thomas Janka
Max-Planck-Institut für Astrophysik
Karl-Scharzschild-Str. 1, 85741 Garching, Germany

ABSTRACT

The neutrino flux and spectra formation in a supernova core is studied by using a Monte Carlo code. The dominant opacity contribution for ν_μ is elastic scattering on nucleons $\nu_\mu \mathrm{N} \to \mathrm{N}\nu_\mu$, where ν_μ always stands for either ν_μ or ν_τ. In addition we switch on or off a variety of processes which allow for the exchange of energy or the creation and destruction of neutrino pairs, notably nucleon bremsstrahlung $\mathrm{NN} \to \mathrm{NN}\nu_\mu\bar\nu_\mu$, the pair annihilation processes $\mathrm{e}^+\mathrm{e}^- \to \nu_\mu\bar\nu_\mu$ and $\nu_\mathrm{e}\bar\nu_\mathrm{e} \to \nu_\mu\bar\nu_\mu$, recoil in elastic nucleon scattering, elastic scattering on electrons $\nu_\mu \mathrm{e}^\pm \to \mathrm{e}^\pm\nu_\mu$ and elastic scattering on electron neutrinos and anti-neutrinos $\nu_\mu\nu_\mathrm{e} \to \nu_\mathrm{e}\nu_\mu$ and $\nu_\mu\bar\nu_\mathrm{e} \to \bar\nu_\mathrm{e}\nu_\mu$. The least important processes are neutrino-neutrino scattering and $\mathrm{e}^+\mathrm{e}^-$ annihilation. The formation of the spectra and fluxes is dominated by the nucleonic processes, i.e. bremsstrahlung and elastic scattering with recoil, but also $\nu_\mathrm{e}\bar\nu_\mathrm{e}$ annihilation and $\nu_\mu \mathrm{e}^\pm$ scattering contribute on a significant level. When all processes are included, the spectral shape of the emitted neutrino flux is always "pinched" and can be represented by a nominal Fermi-Dirac function with an effective degeneracy parameter in the range 1–2, depending on the details of the background model. In all of our cases we find that the average ν_μ and $\bar\nu_\mu$ energy exceeds the average $\bar\nu_\mathrm{e}$ energy by only a small amount, 10% being a typical number. Depending on the density, temperature, and composition profile, the flavor-dependent luminosities L_{ν_e}, $L_{\bar\nu_\mathrm{e}}$, and L_{ν_μ} can mutually differ from each other by up to a factor of two in either direction.

Subject headings: diffusion — neutrinos — supernovae: general

1. INTRODUCTION

In numerical core-collapse supernova (SN) simulations, the transport of μ- and τ-neutrinos has received scant attention because their exact fluxes and spectra are probably not crucial for the explosion mechanism. However, the recent experimental evidence for neutrino oscillations implies that the flavor-dependent fluxes and spectra emitted by a SN will be partly swapped so that at any distance from the source the actual fluxes and spectra can be very different from those originally produced. In principle, this effect can be important for the SN shock revival (Fuller et al. 1992) and r-process nucleosynthesis (Qian et al. 1993), although the experimentally favored small neutrino mass differences suggest that this is not the case. On the other hand, for some of the putative neutrino mixing parameters, notably the large-mixing angle solution of the solar neutrino problem, flavor oscillations are quite relevant for the interpretation of the SN 1987A neutrino signal (Jegerlehner, Neubig, & Raffelt 1996, Lunardini & Smirnov 2001a, Kachelriess et al. 2002, Smirnov, Spergel, & Bahcall 1994). More importantly, the high-statistics neutrino signal from a future galactic SN may allow one to differentiate between some of the neutrino mixing scenarios which explain the presently available data (Chiu & Kuo 2000, Dighe & Smirnov 2000, Dutta et al. 2000, Fuller, Haxton, & McLaughlin 1999, Lunardini & Smirnov 2001b, Minakata & Nunokawa 2001, Takahashi & Sato 2002). Even when the solution of the solar neutrino problem has been settled, the magnitude of the small mixing angle Θ_{13} and the question if the neutrino mass hierarchy is normal or inverted will remain open and can be settled only by future precision measurements at dedicated long-baseline oscillation experiments (Barger et al. 2001, Cervera et al. 2000, Freund, Huber, & Lindner 2001) and/or the observation of a future galactic SN.

The usefulness of SN neutrinos for diagnosing flavor oscillations depends on the flavor dependence of the fluxes and spectra at the source. Very crudely, a SN core is a black-body source of neutrinos of all flavors which are emitted from the surface of the proto-neutron star that was born after collapse. It is the flavor-dependent details of the neutrino transport in the neutron-star atmosphere which cause the spectral and flux differences that can lead to interesting oscillation effects.

The ν_e and $\bar\nu_e$ opacity is dominated by the charged-current processes $\nu_e n \to p e^-$ and $\bar\nu_e p \to n e^+$, reactions that allow for the exchange of energy and lepton number between the medium and the neutrinos. Therefore, it is straightforward to define an energy-dependent neutrinosphere where this reaction freezes out for neutrinos of a particular energy. This sphere yields a thermal contribution to the neutrino flux at the considered energy. The atmosphere of the proto-neutron star is neutron rich, providing for a larger ν_e opacity than for $\bar\nu_e$ so that for a given energy the $\bar\nu_e$ flux originates at deeper and thus hotter layers than the ν_e flux. In other words, a larger fraction of the $\bar\nu_e$ flux emerges with high energies. This simple observation explains the usual hierarchy $\langle\epsilon_{\bar\nu_e}\rangle > \langle\epsilon_{\nu_e}\rangle$ of the mean energies. The spectra are found to be "pinched", meaning that the high-energy tail is suppressed relative to that of a thermal spectrum with the same mean energy (Janka & Hillebrandt 1989a,b). This numerical result can be understood analytically by constructing the neutrino spectrum from the fluxes emitted by the energy-dependent neutrinospheres which are at different temperatures (Myra, Lattimer, & Yahil 1988, Giovanoni, Ellison, & Bruenn 1989).

The formation of the ν_μ, $\bar\nu_\mu$, ν_τ, and $\bar\nu_\tau$ spectra is far more complicated. The opacity is dominated by the neutral-current scattering on nucleons, $\nu_\mu N \to N \nu_\mu$, a process which prevents neutrino free streaming, but is unable to change the neutrino number and is usually considered to be inefficient at exchanging energy. (Here and in the following ν_μ stands for either ν_μ or ν_τ.) Neutrino pairs can be created by nucleon bremsstrahlung, $NN \to NN\nu_\mu\bar\nu_\mu$, and pair annihilation, $e^-e^+ \to \nu_\mu\bar\nu_\mu$ or $\nu_e\bar\nu_e \to \nu_\mu\bar\nu_\mu$, while $\nu_\mu\bar\nu_\mu$ pairs are absorbed by the inverse reactions. In addition, energy is exchanged by elastic scattering on leptons, notably $\nu_\mu e^- \to e^- \nu_\mu$, by the recoil in nucleon scattering, $\nu_\mu N \to N\nu_\mu$, and by inelastic scattering on nucleons $\nu_\mu NN \to NN\nu_\mu$, a channel that is the "crossed process" of bremsstrahlung. For a given neutrino energy these processes freeze out at different radii so that one can define a "number sphere" for the pair processes, an "energy sphere" for the energy-exchange processes, and a "transport sphere" for elastic nucleon scattering with $R_{\rm number} < R_{\rm energy} < R_{\rm transport}$ (Suzuki 1990). The region between the number sphere and the transport sphere plays the role of a *scattering atmosphere* because neutrinos can not be created or destroyed. They propagate by diffusion and can still exchange energy with the background medium.

Usually the ν_μ transport sphere is deeper than the $\bar\nu_e$ sphere so that numerical simulations find $\langle\epsilon_{\nu_\mu}\rangle > \langle\epsilon_{\bar\nu_e}\rangle > \langle\epsilon_{\nu_e}\rangle$. This hierarchy is the main motivation for the proposed use of SN neutrinos as a diagnostic for neutrino oscillations. However, the quantitative statements found in the literature range from $\langle\epsilon_{\nu_\mu}\rangle$ being 20% to nearly a factor of 2 larger than $\langle\epsilon_{\bar\nu_e}\rangle$; for a review see Janka (1993) and Sec. 4.2. Of course, the mean energies and their ratios change significantly between the SN bounce, accretion phase, and the later neutron-star cooling phase. Therefore, one must distinguish carefully between instantaneous fluxes and spectra and the time-integrated values. While for the analysis of the sparse SN 1987A data only time-integrated values make sense, a future galactic SN may well produce enough events to study the instantaneous fluxes and spectra (Barger, Marfatia, & Wood

2001, Minakata et al. 2001).

The overall energy emitted by a SN is often said to be equipartitioned among all six neutrino degrees of freedom. In some numerical simulations the neutrino luminosities are indeed astonishingly equal for all flavors (Totani et al. 1998), while other simulations easily find a factor of two difference between, say, the $\bar{\nu}_\mu$ and $\bar{\nu}_{\rm e}$ luminosities, at least during the accretion phase (Mezzacappa et al. 2001). Therefore, it is by no means obvious how precisely equipartition can be assumed for the purpose of diagnosing neutrino oscillations.

Another important feature is the neutrino spectral shape, notably the amount of pinching. If one could assume with confidence that the instantaneous spectra of all flavors are pinched at the source, and if the measured SN neutrino spectra were instead found to be anti-pinched, this effect would be a powerful diagnostic for the partial spectral swapping caused by flavor oscillations (Dighe & Smirnov 2000).

Unfortunately, the existing literature does not allow one to develop a clear view on these "fine points" of the neutrino fluxes and spectra, largely because not enough attention has been paid to the ν_μ and ν_τ emission from a SN core. The published full numerical SN collapse simulations have not yet included the bremsstrahlung process or nucleon recoils (but see first results of state-of-the-art models in Rampp et al. 2002), even though it is no longer controversial that these effects are important (Janka et al. 1996, Burrows et al. 2000, Hannestad & Raffelt 1998, Raffelt 2001, Suzuki 1991, 1993, Thompson, Burrows, & Horvath 2000). Moreover, some of the interesting information such as the spectral pinching was usually not documented.

Another problem with self-consistent hydrodynamical simulations is that the models with the most elaborate neutrino transport usually do not explode so that even the most recent state-of-the-art simulations do not reach beyond the accretion phase at a few hundred milliseconds after bounce (Rampp & Janka 2000, Mezzacappa et al. 2001), thus not providing any information on the neutron-star cooling phase. Successful multi-dimensional models of the explosion (e.g., Fryer & Warren 2002, Fryer 1999 and references therein) were also not continued to the neutron-star cooling phase. These simulations, moreover, treat the neutrino transport only in a very approximate way and do not provide spectral information. The calculations performed by the Livermore group also yield robust explosions (Totani et al. 1998). They include a mixing-length treatment of the phenomenon of neutron-finger convection in the neutron star, that increases the early neutrino luminosities and thus enhances the energy transfer by neutrinos to the postshock medium (Wilson & Mayle 1993). Whether neutron-finger convection actually occurs inside the neutrinosphere and has effects on a macroscopic scale, however, is an unsettled issue.

We will follow here an alternative approach to full hydrodynamical simulations, i.e. we will study neutrino transport on the background of an assumed neutron-star atmosphere. While this approach lacks hydrodynamical self-consistency, it has the great advantage of allowing one to study systematically the influence of various pieces of microscopic input physics and of the medium profile. The goal is to develop a clearer picture of the generic properties of the SN neutrino spectra and fluxes and what they depend upon.

To this end we have adapted the Monte Carlo code of Janka (1987, 1991) and added new microphysics to it. We go beyond the work of Janka & Hillebrandt (1989a,b) in that we include the bremsstrahlung process, nucleon recoils, $\nu_{\rm e}\bar{\nu}_{\rm e}$ pair annihilation into $\nu_\mu\bar{\nu}_\mu$, and scattering of ν_μ on $\nu_{\rm e}$ and $\bar{\nu}_{\rm e}$. With these extensions we investigate the neutrino transport systematically for a variety of medium profiles that are representative for different SN phases. One of us (Raffelt 2001) has recently studied the ν_μ spectra-formation problem with the limitation to nucleonic processes (elastic and inelastic scattering, recoils, bremsstrahlung), to Maxwell-Boltzmann statistics for the neutrinos, and plane-parallel geometry. Our present study complements this more schematic work by including the leptonic processes, Fermi-Dirac statistics, and spherical geometry. In addition we apply our Monte Carlo code to the transport of $\nu_{\rm e}$ and $\bar{\nu}_{\rm e}$ and thus are able to compare the flavor-dependent fluxes and spectra.

In Sec. 2 we first assess the relative importance of different processes in terms of their energy-dependent "thermalization depth". In this context we introduce a number of stellar background models. In Sec. 3 we perform a Monte Carlo study of ν_μ transport on the previously introduced background models in order to assess the importance of different pieces of input physics. In Sec. 4 we compare the ν_μ fluxes and spectra with those of ν_e and $\bar{\nu}_e$. We conclude in Sec. 5 with a discussion and summary of our findings.

2. THERMALIZATION DEPTH OF ENERGY-EXCHANGE PROCESSES

2.1. Simple Picture of Spectra Formation

One of our goals is to assess the relative importance of different neutrino interaction channels with the background medium of the SN core. As a first step it is instructive to study the thermalization depth of various energy-exchange processes. Within the transport sphere, the neutrinos are trapped by elastic scatterings on nucleons, $\nu_\mu \mathrm{N} \to \mathrm{N}\nu_\mu$, which are by far the most frequent reactions between neutrinos and particles of the stellar medium. (Unless otherwise noted "neutrinos" always refers to any of ν_μ, $\bar{\nu}_\mu$, ν_τ or $\bar{\nu}_\tau$.) Assuming for the moment that these collisions are iso-energetic (no nucleon recoils), it is straightforward to define for a neutrino of given energy ϵ the location ("thermalization depth") where it last exchanged energy with the medium by a reaction such as $\nu_\mu \mathrm{e}^- \to \mathrm{e}^- \nu_\mu$. Following Shapiro & Teukolsky (1983) we define the optical depth for energy exchange or thermalization by

$$\tau_{\rm therm}(r) = \int_r^\infty dr' \sqrt{\frac{1}{\lambda_E(r')}\left[\frac{1}{\lambda_T(r')} + \frac{1}{\lambda_E(r')}\right]}\,. \tag{1}$$

Here, λ_E is the mean free path (mfp) for the relevant energy-exchange process and λ_T the transport mfp, i.e. the mfp corresponding to the cross section for momentum exchange in the $\nu\mathrm{N} \to \mathrm{N}\nu$ reaction. The quantities $\tau_{\rm therm}$, λ_E and λ_T are all understood to depend on the neutrino energy ϵ. The main philosophy of Eq. (1) is that a neutrino trapped by elastic scattering has a chance to exchange energy corresponding to its actual diffusive path through the scattering atmosphere (for a discussion, see Suzuki 1990). The thermalization depth $R_{\rm therm}$ is given by

$$\tau_{\rm therm}(R_{\rm therm}) = \frac{2}{3}\,, \tag{2}$$

where $R_{\rm therm}$ depends on the neutrino energy ϵ.

When this energy dependence is not too steep it makes sense to define an average thermalization depth, i.e. an "energy sphere" that for pair creating processes is equal to the "number sphere." For nucleon bremsstrahlung this requirement is well fulfilled (Raffelt 2001) so that one may picture the energy sphere as a blackbody surface that injects neutrinos into the scattering atmosphere and absorbs those scattered back. The neutrino flux and spectrum emerging from the transport sphere is then easily understood in terms of the energy-dependent transmission probability of the blackbody spectrum launched at the energy sphere. The transport cross section scales as ϵ^2, implying that the transmitted flux spectrum is shifted to lower energies relative to the temperature at the energy sphere. This simple "filter effect" accounts surprisingly well for the emerging flux spectrum (Raffelt 2001). For typical conditions the mean flux energies are 50–60% of those corresponding to the blackbody conditions at the energy sphere.

Moreover, it is straightforward to understand that the effective temperature of the emerging flux spectrum is not overly sensitive to the exact location of the energy sphere. If the energy-exchange reaction is somewhat more effective, the energy sphere is at a larger radius with a lower medium temperature. However, the scattering atmosphere has a smaller optical depth so that the higher-energy neutrinos are less suppressed by the filter effect, partly compensating the smaller energy-sphere temperature. For typical situations Raffelt (2001) found that changing the bremsstrahlung rate by a factor of 3 would change the emerging neutrino energies only by some 10%. This finding suggests that the emitted average neutrino energy is not overly sensitive to the details of the energy-exchange processes.

2.2. Neutron-Star Atmospheres

In order to determine the location of the thermalization depth for different processes we need to define our assumed neutron-star atmospheres. As a first example we use a model taken from a full hydrodynamical simulation. This model is representative for the accretion phase; henceforth we will refer to it as the "Accretion-Phase Model I" (Fig. 1). It was provided to us by O. E. B. Messer and was already used in Raffelt (2001) for a more schematic study. Based on the Woosley & Weaver

Table 1
Characteristics of power-law models.

	Steep	Shallow
p	10	5
q	2.5	1
q/p	0.25	0.2
ρ_0 [10^{14} g cm^{-3}]	2.0	0.2
T_0 [MeV]	31.66	20.0
r_0 [km]	10	10

$15\,M_\odot$ progenitor model labeled s15s7b, the Newtonian collapse simulation was performed with the SN code developed by Mezzacappa et al. (2001). The snapshot is taken at 324 ms after bounce when the shock is at about 120 km, i.e. the star still accretes matter. In this simulation the traditional microphysics for ν_μ transport was included, i.e. iso-energetic scattering on nucleons, e^+e^- annihilation and $\nu_\mu e^-$ scattering.

As another self-consistent example (Accretion-Phase Model II) we obtained a 150 ms postbounce model from M. Rampp (personal communication) that uses a very similar progenitor (s15s7b2). The simulation includes an approximate general relativistic treatment in spherical symmetry as described by Rampp & Janka (2002). The three neutrino flavors are transported with all relevant interactions except $\nu_e\bar{\nu}_e$ pair annihilation to $\nu_\mu\bar{\nu}_\mu$

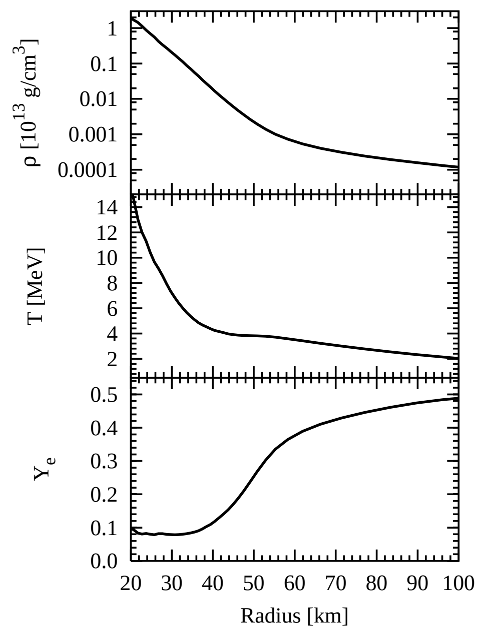

Fig. 1.— Accretion-Phase Model I, a SN model 324 ms after bounce from a Newtonian calculation (O.E.B. Messer, personal communication).

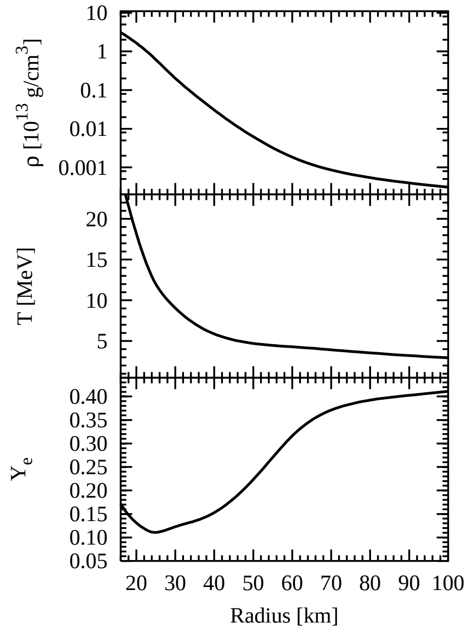

Fig. 2.— Accretion-Phase Model II, a SN core at 150 ms postbounce from a general-relativistic simulation. (M. Rampp, personal communication).

(see also Sec. 4.1 and Rampp et al. 2002).

As another set of examples we use two power-law profiles of the form

$$\rho = \rho_0 \left(\frac{r_0}{r}\right)^p, \quad T = T_0 \left(\frac{r_0}{r}\right)^q, \tag{3}$$

with a constant electron fraction per baryon Y_e. We adjust parameters such that $\langle\epsilon\rangle \approx 20$–25 MeV for the emerging neutrinos to obtain model atmospheres in the ballpark of results from proto-neutron star evolution calculations. We define a "steep" power-law model, corresponding to the one used by Raffelt (2001), and a "shallow" one; the characteristics are given in Table 1. The shallow model could be characteristic of a SN core during the accretion phase while the steep model is more characteristic for the neutron-star cooling phase. The constant electron fraction Y_e is another parameter that allows us to investigate the relative importance of the leptonic processes as a function of the assumed Y_e.

2.3. Thermalization Depth

We now calculate the thermalization depth as a function of the neutrino energy ϵ for several energy-exchanging processes and the neutron-star atmospheres described above. We consider the neutrino mfp for nucleon bremsstrahlung $\mathrm{NN} \to \mathrm{NN}\nu_\mu\bar\nu_\mu$, pair annihilation $\mathrm{e^+e^-} \to \nu_\mu\bar\nu_\mu$ and $\nu_e\bar\nu_e \to \nu_\mu\bar\nu_\mu$, and scattering on charged leptons $\nu_\mu \mathrm{e}^\pm \to \mathrm{e}^\pm\nu_\mu$. The numerical implementation of the reaction rates is described in Appendix B.

In Figs. 3 and 4 we give the thermalization depth $R_{\rm therm}$ as a function of neutrino energy ϵ for the two hydrodynamically self-consistent accretion-phase models. From top to bottom the panels show the results for ν_e, $\bar\nu_e$, and ν_μ, respectively. The step-like curves represent the temperature profiles in terms of the mean neutrino energy, $\langle\epsilon_\nu\rangle = 3.15\,T$ for non-degenerate neutrinos at the local medium temperature; the steps correspond to the radial zones of our Monte Carlo simulation. The other curves represent $R_{\rm therm}$ for bremsstrahlung (b), $\mathrm{e^+e^-}$ annihilation (p), $\nu_e\bar\nu_e$ annihilation (n), and scattering on $\mathrm{e}^\pm$ (s). In the case of ν_e and $\bar\nu_e$ we do not include bremsstrahlung and $\nu_e\bar\nu_e$ annihilation. Particle creation is in this case largely dominated by the charged current reactions on nucleons (urca).

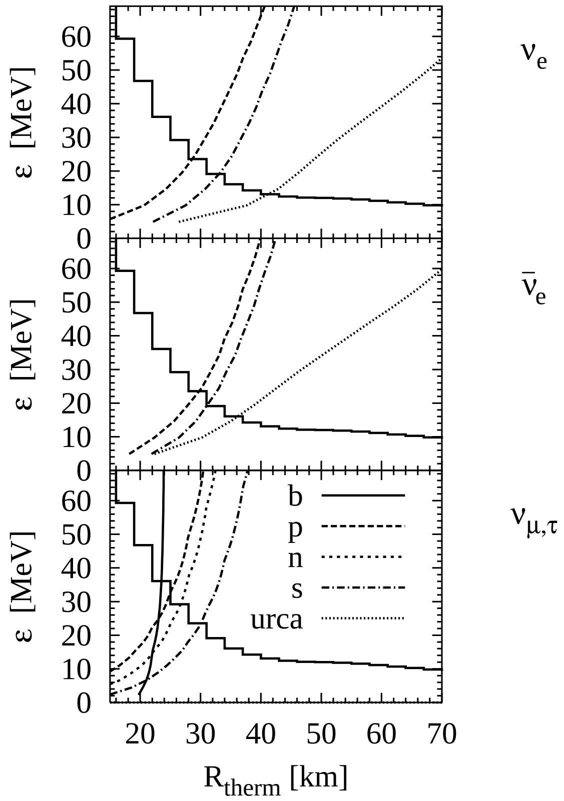

Fig. 3.— $R_{\rm therm}$ as a function of neutrino energy ϵ for our Accretion-Phase Model I. From top to bottom the panels show the results for ν_e, $\bar\nu_e$, and ν_μ. Energy exchanging processes: bremsstrahlung (solid line), $\mathrm{e^+e^-}$ annihilation (dashed), $\nu_e\bar\nu_e$ annihilation (dotted), and scattering on $\mathrm{e}^\pm$ (dash-dotted). "Urca" denotes the charged-current reaction of ν_e and $\bar\nu_e$ on nucleons. The steps represent $\langle\epsilon\rangle = 3.15\,T$.

For the power-law models we show $R_{\rm therm}$ for ν_μ in Figs. 5 and 6. The different panels correspond to the indicated values of the electron fraction Y_e. Note that Y_e represents the net electron density per baryon, i.e. the e^- density minus that of e^+ so that $Y_e = 0$ implies that there is an equal thermal population of e^- and e^+.

The ν_μ absorption rate for the bremsstrahlung process varies approximately as ϵ^{-1}, the $\nu_\mu\mathrm{N}$ transport cross section as ϵ^2 so that the inverse mfp for thermalization varies only as $\epsilon^{1/2}$. This explains why $R_{\rm therm}$ for bremsstrahlung is indeed quite independent of ϵ. Therefore, bremsstrahlung

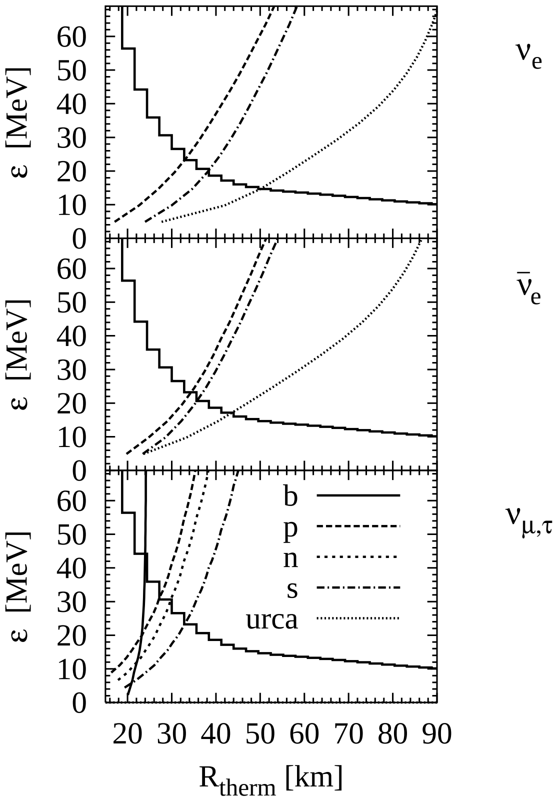

Fig. 4.— Same as Fig. 3 for the Accretion-Phase Model II.

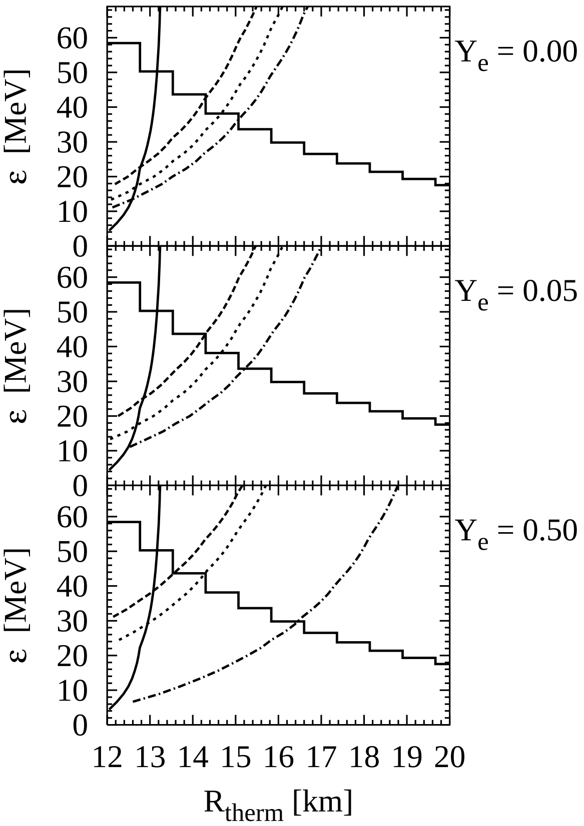

Fig. 5.— $R_{\rm therm}$ for ν_μ in the steep power-law model with the indicated values of $Y_{\rm e}$. This figure corresponds to the bottom panel of Fig. 3.

alone allows one to specify a rather well-defined energy sphere. The other processes depend much more sensitively on ϵ so that a mean energy sphere is much less well defined.

Both electron scattering and the leptonic pair processes are so ineffective at low energies that true local thermodynamic equilibrium (LTE) can not be established even for astonishingly deep locations. Bremsstrahlung easily "plugs" this low-energy hole so that one can indeed expect LTE for all relevant neutrino energies below a certain radius. For higher energies, the leptonic processes dominate and shift the energy sphere to larger radii than bremsstrahlung alone. The relative importance of the various processes depends on the density and temperature profiles as well as $Y_{\rm e}$.

In order to assess the role of the various processes for the overall spectra formation one needs to specify some typical neutrino energy. One possibility would be $\langle\epsilon\rangle$ for neutrinos in LTE. Another possibility is the mean energy of the neutrino flux, in particular the mean energy of those neutrinos which actually leave the star. For our power-law atmospheres this is always around 20–25 MeV. Therefore, the process with the largest $R_{\rm therm}$ in this energy band is the one most relevant for determining the emerging neutrino spectrum. It appears that at least for steep profiles pair annihilation is never crucial once bremsstrahlung is included, i.e. we would guess that including pair annihilation will not affect the emerging neutrino spectra. The relevance of electron scattering is far more difficult to guess. On the one hand it surely is more important than recoil in nucleon scatterings for some of the relevant energies, on the other hand we are not able to define an energy sphere for nucleon recoils because this process is different from the others in that neutrinos transfer only a small fraction of their energy per scatter-

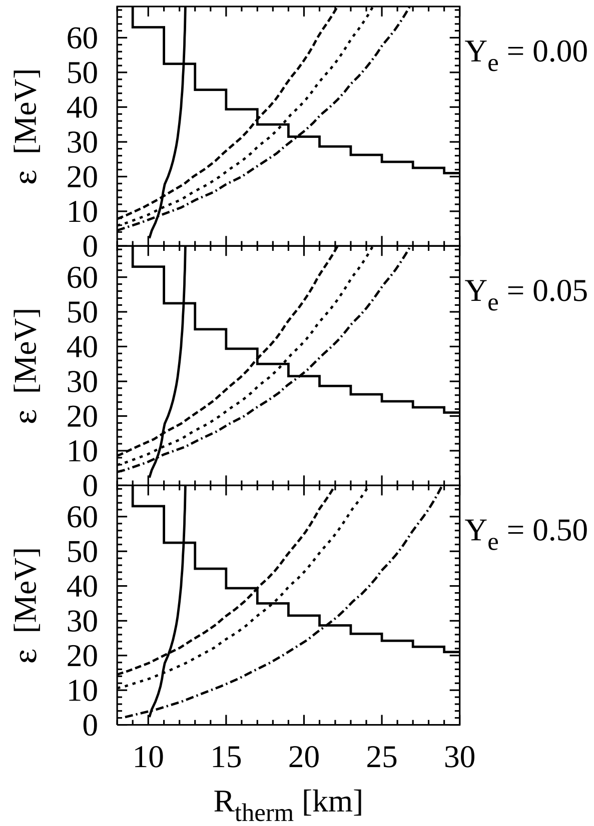

Fig. 6.— Same as Fig. 5 for the shallow power-law model.

ing. Therefore, it is not straightforward to assess the relevance of electron scattering compared with nucleon recoils on the basis of the various thermalization spheres alone.

3. MONTE CARLO STUDY OF MUON NEUTRINO TRANSPORT

3.1. Spectral Characteristics

In order to characterize the neutrino spectra and fluxes emerging from a neutron star we need to introduce some simple and intuitive parameters. One is the mean energy

$$\langle\epsilon\rangle = \frac{\int_0^\infty d\epsilon\,\epsilon\,\int_{-1}^{+1} d\mu\, f(\epsilon,\mu)}{\int_0^\infty d\epsilon\,\int_{-1}^{+1} d\mu\, f(\epsilon,\mu)}\,, \tag{4}$$

where $f(\epsilon,\mu)$ is the neutrino distribution function with ϵ the energy and μ the cosine of the angle between the neutrino momentum and the radial direction. If the neutrinos are in LTE without a chemical potential one has

$$f(\epsilon,\mu) = \frac{\epsilon^2}{1+\exp(\epsilon/T)} \tag{5}$$

and therefore

$$\langle\epsilon\rangle = \frac{7\pi^4}{180\,\zeta_3}\,T \approx 3.1514\,T\,. \tag{6}$$

One can define an effective neutrino temperature for non-equilibrium distributions by inverting this relationship.

It is often useful to extract spectral characteristics for those neutrinos which are actually flowing by removing the isotropic part of the distribution. Specifically, we define the average flux energy by

$$\langle\epsilon\rangle_{\rm flux} = \frac{\int_0^\infty d\epsilon\,\epsilon\,\int_{-1}^{+1} d\mu\,\mu\, f(\epsilon,\mu)}{\int_0^\infty d\epsilon\,\int_{-1}^{+1} d\mu\,\mu\, f(\epsilon,\mu)}\,. \tag{7}$$

Far away from the star all neutrinos will flow essentially in the radial direction, implying that the angular distribution becomes a delta-function in the forward direction so that $\langle\epsilon\rangle_{\rm flux} = \langle\epsilon\rangle$. However, in the trapping regions the two averages are very different because the distribution function is dominated by its isotropic term.

To characterize the spectrum beyond the mean energy one can consider a series of moments $\langle\epsilon^n\rangle$ (Janka & Hillebrandt 1989a); we usually limit ourselves to $n = 1$ and 2. Note that a Fermi-Dirac distribution at zero chemical potential yields

$$a \equiv \frac{\langle\epsilon^2\rangle}{\langle\epsilon\rangle^2} = \frac{486000\,\zeta_3\zeta_5}{49\,\pi^8} \approx 1.3029\,. \tag{8}$$

For a Maxwell-Boltzmann distribution this quantity would be 4/3. Following Raffelt (2001) we further define the "pinching parameter"

$$p \equiv \frac{1}{a}\,\frac{\langle\epsilon^2\rangle}{\langle\epsilon\rangle^2}\,, \tag{9}$$

where $p = 1$ signifies that the spectrum is thermal up to its second moment, while $p < 1$ signifies a pinched spectrum (high-energy tail suppressed), $p > 1$ an anti-pinched spectrum (high-energy tail enhanced). An analogous definition applies to the pinching parameter $p_{\rm flux}$ of the flux spectrum by replacing $\langle\cdot\rangle$ with $\langle\cdot\rangle_{\rm flux}$.

We will find that when all energy-transfer mechanisms are included, the flux spectra are always pinched. In this case it makes sense to approximate the spectrum as a nominal Fermi-Dirac distribution characterized by a temperature T and a degeneracy parameter η according to

$$f(\epsilon) = \frac{\epsilon^2}{1 + \exp\left(\frac{\epsilon}{T} - \eta\right)} \qquad (10)$$

(Janka & Hillebrandt 1989a). In Fig. 7 we show $\langle \epsilon/T \rangle$ and p as a function of η. Up to second order, expansions are

$$\begin{aligned} \langle \epsilon/T \rangle &\approx 3.1514 + 0.1250\,\eta + 0.0429\,\eta^2 \\ p &\approx 1 - 0.0174\,\eta - 0.0046\,\eta^2\,. \end{aligned} \qquad (11)$$

These expansions are also shown in Fig. 7 as dashed lines.

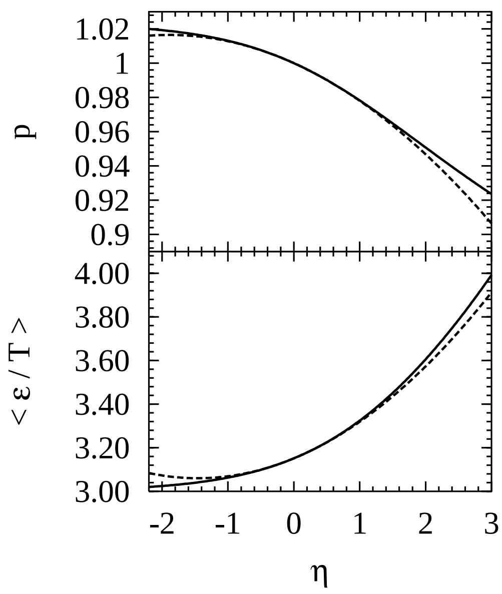

Fig. 7.— Mean energy and pinching parameter as a function of the degeneracy parameter for a Fermi-Dirac distribution. As dashed lines we show the expansions given in Eq. (11).

In some publications the root-mean-square energy $\langle \epsilon \rangle_{\rm rms}$ is given instead of the average energy. The definition corresponding to Eq. (4) is

$$\langle \epsilon \rangle_{\rm rms} = \sqrt{\frac{\int_0^\infty d\epsilon \int_{-1}^{+1} d\mu\, \epsilon^3 f(\epsilon,\mu)}{\int_0^\infty d\epsilon \int_{-1}^{+1} d\mu\, \epsilon\, f(\epsilon,\mu)}} = \sqrt{\frac{\langle \epsilon^3 \rangle}{\langle \epsilon \rangle}}\,. \qquad (12)$$

This characteristic spectral energy is useful for estimating the energy transfer from neutrinos to the stellar medium in reactions with cross sections proportional to ϵ^2. For thermal neutrinos with vanishing chemical potential we find

$$\langle \epsilon \rangle_{\rm rms} = \sqrt{\frac{930}{441}}\,\pi\, T \approx 4.5622\, T\,. \qquad (13)$$

With Eq. (6) this corresponds to $\langle \epsilon \rangle \approx 0.691 \langle \epsilon \rangle_{\rm rms}$.

3.2. Monte Carlo Set Up

We have run our Monte Carlo code, that is described in Appendix A, for the stellar background models introduced in Sec. 2.2 and for different combinations of energy-changing neutrino reactions. Our main interest is to assess the impact of the scattering atmosphere on the flux and spectrum formation. Therefore, it is sufficient to simulate the neutrino transport above some radius where we have to specify a boundary condition.

We always use a blackbody boundary condition at the bottom of the atmosphere, i.e. we assume neutrinos to be in LTE at the local temperature and the appropriate chemical potential; for ν_μ and ν_τ the latter is taken to vanish. As a consequence of this boundary condition, the luminosity emerging at the surface is generated within the computational domain and calculated by our Monte Carlo transport. A small flux across the inner boundary develops because of the negative gradients of temperature and density in the atmosphere, but its magnitude depends on the radial resolution of the neutron-star atmosphere and will not in general correspond to the physical diffusive flux. But as long as the flux is small compared to the luminosity at the surface, the emerging neutrino spectra will not depend on the lower boundary condition. Usually it is sufficient to place the inner grid radius deeper in the star than the thermalization depth of the dominant pair process.

The shallow energy dependence of the thermalization depth of the nucleon bremsstrahlung implies that whenever we include this process it is not difficult to choose a reasonable location for the lower boundary. Taking the latter too deep in the star is very CPU-expensive as one spends most of the simulation for calculating frequent scatterings of neutrinos that are essentially in LTE.

We always include ν_μN scattering as the main opacity source. For energy exchange, we switch on or off bremsstrahlung (b), nucleon recoil (r), scattering on electrons (s), e^+e^- pair annihilation (p), and $\nu_e\bar{\nu}_e$ annihilation (n). We never include inelastic nucleon scattering $\nu_\mu NN \to NN\nu_\mu$ as this process is never important relative to recoil (Raffelt 2001). Likewise, we ignore scattering on ν_e and $\bar{\nu}_e$ which is always unimportant if $\nu_\mu e^\pm$ is included (Buras et al. 2002). We also neglect $\nu_\mu\nu_\mu$ or $\nu_\mu\bar{\nu}_\mu$ scattering even though such processes may have a larger rate than some of the included leptonic processes. Processes of this type do not exchange energy between the neutrinos and the background medium. They are therefore not expected to affect the emerging fluxes and should also have a minor effect on the emitted spectra.

3.3. Importance of Different Processes

3.3.1. Accretion-Phase Model I

Our first goal is to assess the relative importance of different energy-exchange processes for the ν_μ transport. As a first example we begin with our Accretion-Phase Model I. The results from our numerical runs are summarized in Table 2 where for each run we give $\langle\epsilon\rangle_{\rm flux}$, $\langle\epsilon^2\rangle_{\rm flux}$, and the pinching parameter $p_{\rm flux}$ for the emerging flux spectrum, the temperature and degeneracy parameter of an effective Fermi-Dirac spectrum producing the same first two energy moments, and the luminosity.

The first row contains the muon neutrino flux characteristics of the original Boltzmann transport calculation by Messer. To make a connection to these results we ran our code with the same input physics, i.e. $\nu_\mu e^\pm$ scattering (s) and e^+e^- annihilation (p). There remain small differences between the original spectral characteristics and ours. These can be caused by differences in the implementation of the neutrino processes, by the limited number of energy and angular bins in the Boltzmann solver, the coarser resolution of the radial grid in our Monte Carlo runs, and by our simple blackbody lower boundary condition. We interpret the first two rows of Table 2 as agreeing sufficiently well with each other that a detailed understanding of the differences is not warranted. Henceforth we will only discuss differential effects within our own implementation.

In the next row (bsp) we include nucleon bremsstrahlung which has the effect of increasing the luminosity by a sizable amount without affecting much the spectral shape. This suggests that bremsstrahlung is important as a source for $\nu_\mu\bar{\nu}_\mu$ pairs, but that the spectrum is then shaped by the energy-exchange in scattering with $e^\pm$. In the next row we switch off $e^\pm$ scattering (bp) so that no energy is exchanged except by pair-producing processes. The spectral energy indeed increases significantly. However, the biggest energy-exchange effect in the scattering regime is nucleon recoil. In the next two rows we include recoil (brp) and then additionally $e^\pm$ scattering (brsp), both lowering the spectral energies and also the luminosities.

The picture of all relevant processes is completed by adding $\nu_e\bar{\nu}_e$ pair annihilation (brspn), which is similar to e^+e^- pair annihilation, but a factor of 2–3 more important (Buras et al. 2002). The luminosity is again increased, an effect which is understood in terms of our blackbody picture for the number and energy spheres. In the lower panel of Fig. 3 we see that $R_{\rm therm}$ moves to larger radii once "n" is switched on, the radiating surface of the "blackbody" increases and more pairs are emitted. For both "p" and "n" $R_{\rm therm}$ is strongly energy dependent and therefore it is impossible to define a sharp thermalization radius.

To study the relative importance of the different pair processes, we switch off the leptonic ones (row "brs") and compare this to only the leptonic processes (row "rspn"). In this stellar model both types contribute significantly. Comparing then "brsp" with "brsn" shows that among the leptonic processes "n" is clearly more important than "p".

The last row "brsnpn" includes in addition to all other processes scattering on ν_e and $\bar{\nu}_e$. It was already shown by Buras et al. (2002) that this process is about half as important as scattering on $e^\pm$ and its influence on the neutrino flux and spectra is negligible. We show this case for completeness but do not include scattering on ν_e and $\bar{\nu}_e$ for any of our further models.

3.3.2. Steep Power Law

As another example we study the steep power-law model defined in Eq. (3) and Table 1. This model is supposed to represent the outer layers of a late-time proto-neutron star but without being hydrostatically self-consistent. It connects directly with Raffelt (2001), where the same pro-

Table 2
Monte Carlo results for Accretion-Phase Model I.

Energy exchange					$\langle\epsilon\rangle_{\rm flux}$	$\langle\epsilon^2\rangle_{\rm flux}$	$p_{\rm flux}$	T	η	L_ν
original run					17.5	388.	0.97	5.2	1.1	14.4
–	–	s	p	–	16.6	362.	1.01	5.3	−0.3	15.8
b	–	s	p	–	16.3	351.	1.02	5.4	−2.2	19.1
b	–	–	p	–	17.8	419.	1.02	5.9	−1.9	20.1
b	r	–	p	–	15.1	285.	0.96	4.3	1.6	18.6
b	r	s	p	–	14.2	255.	0.98	4.2	1.1	14.8
b	r	s	p	n	14.4	264.	0.97	4.3	1.2	17.6
–	–	s	p	n	16.9	369.	0.99	5.3	0.4	20.2
b	r	s	–	–	14.0	251.	0.99	4.3	0.6	13.1
b	r	s	–	n	14.4	263.	0.97	4.3	1.2	17.0
–	r	s	p	–	14.5	265.	0.97	4.3	1.2	13.0
–	r	s	p	n	14.7	269.	0.96	4.2	1.7	16.8
b	r	sn	p	n	14.3	260.	0.97	4.3	1.2	17.9

Note.—For energy exchange, "b" refers to bremsstrahlung, "r" to recoil, "s" to scattering on electrons and positrons, "p" to e^+e^- annihilation, "n" to $\nu_e\bar{\nu}_e$ annihilation, and "sn" to scattering on both $e^\pm$ and ν_e, $\bar{\nu}_e$. We give $\langle\epsilon\rangle_{\rm flux}$ and T in MeV, $\langle\epsilon^2\rangle_{\rm flux}$ in MeV^2, and L_ν in 10^{51} erg s^{-1}.

file was used in a plane parallel setup, studying bremsstrahlung and nucleon recoil. The results of our runs are displayed in Table 3 and agree very nicely with those obtained by Raffelt (2001), corresponding to our cases "b" and "br".

For investigating the importance of leptonic processes, we run our code with a variety of neutrino interactions and in addition assume a constant electron fraction Y_e throughout the whole stellar atmosphere. This assumption is somewhat artificial, but gives us the opportunity to study extreme cases in a controlled way. In the relevant region $Y_\mathrm{e} = 0.5$ yields the highest possible electron density. In addition we study the electron fraction being one order of magnitude smaller, $Y_\mathrm{e} = 0.05$, and finally the extreme case with an equal number of electrons and positrons, $Y_\mathrm{e} = 0$.

The first leptonic process we consider is $\mathrm{e}^+\mathrm{e}^-$ pair annihilation. Comparing the rows "bp" with the row "b" shows a negligible effect on the spectrum, but a rise in luminosity. Increasing Y_e brings the luminosity almost back to the "b" case, because the electron degeneracy rises and the positron density decreases so that the pair process becomes less important.

Adding scattering on $\mathrm{e}^\pm$ forces the transported neutrinos to stay closer to the medium temperature, i.e. reduces their mean energy. Of course, the scattering rate increases with the number of electrons and positrons, i.e. for higher Y_e we get lower spectral energies. For the luminosity the situation is more complicated. Since the neutrino flux energies decrease when we switch on $\mathrm{e}^\pm$ scattering we would expect a lower luminosity. However, the opacity of the medium to neutrinos is strongly energy dependent and low energy neutrinos can escape more easily than high-energy ones, increasing the number flux. On balance, the "bsp" luminosities are larger compared to the "bp" ones.

To compare the scattering on $\mathrm{e}^\pm$ with the one on nucleons, we turn off "s" again and instead switch on recoil (r). Qualitatively, the energy exchange is very different from the earlier case. In the scattering on $\mathrm{e}^\pm$ a neutrino can exchange a large amount of energy, while for scattering on nucleons the energy exchange is small. But since neutrino-nucleon scattering is the dominant source of opacity that keeps the neutrinos inside the star, the scatterings are very frequent. This leads to a stronger suppression in the high-energy tail of the neutrino spectrum and therefore to a visibly smaller mean flux energy and lower effective spectral temperature, but higher effective degeneracy. Many nucleon scatterings, however, are needed to downgrade the high-energy neutrinos (different from $\mathrm{e}^\pm$ scattering). Therefore neutrinos stay longer at high energies and experience a larger opacity and a larger amount of backscattering. This suppresses the neutrino flux significantly.

In the runs including both scattering reactions (brsp), we find a mixture of the effects of $\mathrm{e}^\pm$ and nucleon scatterings and an enhanced reduction of the mean flux energy.

Finally, adding the neutrino pair process yields almost no change in energy and pinching, but an increased luminosity as expected from the analogous case in Sec. 3.3.1. Although this profile is rather steep, leptonic pair processes are still important (Fig. 5).

In order to estimate the sensitivity to the exact treatment of nucleon bremsstrahlung we have performed one run with the bremsstrahlung rate artificially enhanced by a factor of 3, and one where it was decreased by a factor 0.3. All other processes were included. The emerging fluxes and spectra indeed do not depend sensitively on the exact strength of bremsstrahlung.

3.3.3. Shallow power law

For the shallow power law almost the same discussion as for the steep case applies. As we can already infer from Fig. 6, leptonic processes are more important. This leads to a much higher increase of the neutrino flux once "p" or "n" are included, and to stronger spectral pinching when $\mathrm{e}^+\mathrm{e}^-$ annihilation is switched on. Scattering on $\mathrm{e}^\pm$ downgrades the transported neutrino flux by a larger amount.

3.4. Summary

We find that the ν_μ spectra are reasonably well described by the simple picture of a blackbody sphere determined by the thermalization depth of the nucleonic bremsstrahlung process, the "filter effect" of the scattering atmosphere, and energy transfers by nucleon recoils. This is also true for the ν_μ flux in case of steep neutron-star atmospheres. For more shallow atmospheres pair anni-

Table 3

Monte Carlo results for the steep power-law model.

Energy exchange					Y_e	$\langle\epsilon\rangle_{\rm flux}$	$\langle\epsilon^2\rangle_{\rm flux}$	$p_{\rm flux}$	T	η	L_ν
b	–	–	–	–	—	25.8	962.	1.11	—	—	21.0
b	r	–	–	–	—	19.5	487.	0.98	6.0	0.7	14.5
b	–	–	p	–	0	25.4	890.	1.06	—	—	23.8
b	–	–	p	–	0.05	25.6	908.	1.06	—	—	23.2
b	–	–	p	–	0.5	25.5	917.	1.08	—	—	21.6
b	–	s	p	–	0	24.2	787.	1.03	—	—	24.5
b	–	s	p	–	0.05	23.8	753.	1.02	—	—	24.5
b	–	s	p	–	0.5	21.3	591.	1.00	6.8	−0.3	23.1
b	r	–	p	–	0.5	20.0	507.	0.98	6.0	1.0	16.8
b	r	s	p	–	0	20.3	518.	0.97	5.9	1.4	19.7
b	r	s	p	–	0.05	20.3	518.	0.97	5.9	1.4	19.5
b	r	s	p	–	0.5	19.6	488.	0.98	5.9	1.1	18.7
b	r	s	p	n	0	20.7	535.	0.96	5.8	1.8	23.9
b×3	r	s	p	n	0.05	20.3	522.	0.97	6.0	1.3	24.2
b	r	s	p	n	0.05	20.6	530.	0.96	5.9	1.7	23.8
b×0.3	r	s	p	n	0.05	20.7	534.	0.96	5.8	1.8	23.4
b	r	s	p	n	0.5	19.8	499.	0.97	5.9	1.2	21.4

Table 4

Monte Carlo results for the shallow power-law model.

Energy exchange					Y_e	$\langle\epsilon\rangle_{\rm flux}$	$\langle\epsilon^2\rangle_{\rm flux}$	$p_{\rm flux}$	T	η	L_ν
b	–	–	–	–	—	27.7	1120.	1.12	—	—	20.3
b	r	–	–	–	—	20.1	521.	0.99	6.3	0.4	13.4
b	–	–	p	–	0	27.7	974.	0.98	8.3	1.0	43.1
b	–	–	p	–	0.05	27.9	990.	0.98	8.3	1.1	43.3
b	–	–	p	–	0.5	28.3	1019.	0.98	8.5	1.0	38.3
b	–	s	p	–	0	25.5	830.	0.98	7.6	1.1	46.2
b	–	s	p	–	0.05	25.4	815.	0.97	7.5	1.2	46.3
b	–	s	p	–	0.5	23.5	706.	0.98	7.1	1.0	44.8
b	r	–	p	–	0.5	22.5	624.	0.95	6.1	2.2	33.1
b	r	s	p	–	0	22.3	612.	0.95	6.1	2.1	39.6
b	r	s	p	–	0.05	22.2	609.	0.95	6.1	2.1	39.1
b	r	s	p	–	0.5	21.7	585.	0.95	6.1	1.9	39.2
b	r	s	p	n	0	22.2	608.	0.94	6.0	2.2	54.7
b	r	s	p	n	0.05	22.4	615.	0.94	6.1	2.3	54.9
b	r	s	p	n	0.5	21.8	587.	0.95	6.1	1.9	51.3

hilation (e^+e^- and $\nu_e\bar{\nu}_e$), however, yields a large contribution to the emitted ν_μ flux and $e^\pm$ scattering reduces the mean flux energy significantly. It is therefore important for state-of-the art transport calculations to include these leptonic processes. The traditional process $e^+e^- \to \nu_\mu\bar{\nu}_\mu$ is subdominant compared to $\nu_e\bar{\nu}_e \to \nu_\mu\bar{\nu}_\mu$ annihilation as previously found by Buras et al. (2002). The relative importance of the various reactions depends on the stellar profile.

Neutrinos emitted from a blackbody surface and filtered by a scattering atmosphere without recoils and leptonic processes have an anti-pinched spectrum (Raffelt 2001). However, after all energy-exchanging reactions have been included we find that the spectra are always pinched. When described by effective Fermi-Dirac distributions, the nominal degeneracy parameter η is typically in the range 1–2, depending on the profile and electron concentration.

4. COMPARING DIFFERENT FLAVORS

4.1. Monte Carlo Study

The new energy-exchange channels studied in the previous section lower the average ν_μ energies. In order to compare the ν_μ fluxes and spectra with those of ν_e and $\bar{\nu}_e$ we perform a new series of runs where we include the full set of relevant microphysics for ν_μ and also simulate the transport of ν_e and $\bar{\nu}_e$.

The microphysics for the interactions of ν_e and $\bar{\nu}_e$ is the same as in Janka & Hillebrandt (1989a,b), i.e. charged-current reactions of $e^\pm$ with nucleons, iso-energetic scattering on nucleons, scattering on $e^\pm$, and e^+e^- pair annihilation. In principle one should also include nucleon bremsstrahlung and the effect of nucleon recoils for the transport of ν_e and $\bar{\nu}_e$, but their effects will be minimal. Therefore, we preferred to leave the original working code unmodified for these flavors.

In the first three rows of Table 5 we give the spectral characteristics for the Accretion-Phase Model I from the original simulation of Messer. The usual hierarchy of average neutrino energies is found, i.e. $\langle\epsilon_{\nu_e}\rangle : \langle\epsilon_{\bar{\nu}_e}\rangle : \langle\epsilon_{\nu_\mu}\rangle = 0.86 : 1 : 1.20$. The luminosities are essentially equal between $\bar{\nu}_e$ and ν_e while ν_μ, $\bar{\nu}_\mu$, ν_τ, and $\bar{\nu}_\tau$ each provide about half of the $\bar{\nu}_e$ luminosity.

Our Monte Carlo runs of this profile establish the same picture for the same input physics. Although our mean energies are slightly offset to lower values for all flavors relative to the orginial run, our energies relative to each other are $\langle\epsilon_{\nu_e}\rangle : \langle\epsilon_{\bar{\nu}_e}\rangle : \langle\epsilon_{\nu_\mu}\rangle = 0.84 : 1 : 1.19$ and thus very similar. However, once we include all energy exchanging processes we find $0.84 : 1 : 1.02$ instead. Therefore, $\langle\epsilon_{\nu_\mu}\rangle$ no longer exceeds $\langle\epsilon_{\bar{\nu}_e}\rangle$ by much. The luminosity of ν_μ is about half that of ν_e or $\bar{\nu}_e$ which are approximately equal, in rough agreement with the original results. Even though the additional processes lower the mean energy of ν_μ they yield a more than 10% higher ν_μ luminosity, mainly due to $\nu_e\bar{\nu}_e$ annihilation.

As another example of an accreting protoneutron star we use the Accretion-Phase Model II. The neutrino interactions included in this model were nucleon bremsstrahlung, scattering on $e^\pm$, and e^+e^- annihilation. Nucleon correlations, effective mass, and recoil were taken into account, following Burrows & Sawyer (1998, 1999), as well as weak magnetism effects (Horowitz 2002) and quenching of g_A at high densities (Carter & Prakash 2002). All these improvements to the traditional microphysics affect mainly ν_μ and to some degree also $\bar{\nu}_e$. Weak magnetism terms decrease the nucleon scattering cross sections for $\bar{\nu}_\mu$ more strongly than they modify ν_μ scatterings. In this hydrodynamical calculation, however, ν_μ and $\bar{\nu}_\mu$ were treated identically by using the average of the corresponding reaction cross sections. The effects of weak magnetism on the transport of ν_μ and $\bar{\nu}_\mu$ are therefore not included to very high accuracy. Note, moreover, that the original data come from a general relativistic hydrodynamical simulation with the solution of the Boltzmann equation for neutrino transport calculated in the comoving frame of the stellar fluid. Therefore the neutrino results are affected by gravitational redshift and, depending on where they are measured, may also be blueshifted by Doppler effects due to the accretion flow to the nascent neutron star.

Our Monte Carlo simulation in contrast was performed on a static background without general relativistic corrections. It includes bremsstrahlung, recoil, e^+e^- pair annihilation, scattering on $e^\pm$, and $\nu_e\bar{\nu}_e$ annihilation, i.e. our microphysics is similar but not identical with that used in the original run. As an outer radius we took 100 km; all

Table 5
Comparing Monte Carlo results for different flavors.

Model and Flavor	Y_e	$\langle\epsilon\rangle_{\rm flux}$	$\frac{\langle\epsilon\rangle_{\rm flux}}{\langle\epsilon_{\bar\nu_e}\rangle_{\rm flux}}$	$\langle\epsilon^2\rangle_{\rm flux}$	$p_{\rm flux}$	T	η	L_ν
Accretion-Phase Model I								
Original								
ν_μ, $\bar\nu_\mu$	—	17.5	1.20	388.	0.97	5.2	1.1	14.4
$\bar\nu_e$	—	14.6	1	253.	0.91	3.5	3.4	29.2
ν_e	—	12.5	0.86	190.	0.93	3.2	2.8	30.8
Our runs								
ν_μ, $\bar\nu_\mu$ ("sp")	—	16.6	1.19	362.	1.01	5.3	−0.3	15.8
ν_μ, $\bar\nu_\mu$ (all processes)	—	14.3	1.02	260.	0.97	4.3	1.2	17.9
$\bar\nu_e$	—	14.0	1	237.	0.93	3.6	2.7	31.7
ν_e	—	11.8	0.84	175.	0.97	3.4	1.4	31.9
Accretion-Phase Model II								
Original								
ν_μ, $\bar\nu_\mu$	—	17.2	1.09	380.	0.98	5.2	0.8	32.4
$\bar\nu_e$	—	15.8	1	300.	0.92	4.0	3.0	68.1
ν_e	—	12.9	0.82	207.	0.96	3.7	1.7	65.6
Our runs								
ν_μ, $\bar\nu_\mu$	—	15.7	1.02	317.	0.98	4.8	0.8	27.8
$\bar\nu_e$	—	15.4	1	283.	0.92	3.8	3.2	73.5
ν_e	—	13.0	0.84	207.	0.95	3.6	2.1	73.9
Steep Power Law $p = 10$								
$q = 2.5$								
ν_μ, $\bar\nu_\mu$	0.15	20.4	1.10	525.	0.96	5.9	1.5	23.5
$\bar\nu_e$	0.15	18.5	1	413.	0.92	4.6	3.0	23.5
ν_e	0.15	12.7	0.69	198.	0.94	3.4	2.4	12.8
ν_μ, $\bar\nu_\mu$	0.2	20.4	1.14	521.	0.97	5.9	1.5	23.3
$\bar\nu_e$	0.2	17.9	1	383.	0.92	4.4	3.1	11.7
ν_e	0.2	13.4	0.75	218.	0.93	3.4	2.9	24.4
$q = 3.0$								
ν_μ, $\bar\nu_\mu$	0.1	17.7	1.14	393.	0.96	5.0	1.8	12.7
$\bar\nu_e$	0.1	15.5	1	289.	0.93	4.0	2.8	8.8
ν_e	0.1	10.5	0.68	132.	0.92	2.6	3.0	6.6
$q = 3.5$								
ν_μ, $\bar\nu_\mu$	0.07	15.8	1.22	310.	0.95	4.4	2.1	7.9
$\bar\nu_e$	0.07	13.0	1	207.	0.94	3.5	2.3	4.3
ν_e	0.07	9.4	0.72	103.	0.90	2.1	3.9	4.1
Shallow Power Law $p = 5$, $q = 1$								
ν_μ, $\bar\nu_\mu$	0.3	22.0	1.14	596.	0.94	6.0	2.2	53.9
$\bar\nu_e$	0.3	19.3	1	440.	0.91	4.5	3.7	85.7
ν_e	0.3	14.7	0.76	262.	0.93	3.8	2.7	56.5

Note.—We give $\langle\epsilon\rangle_{\rm flux}$ and T in MeV, $\langle\epsilon^2\rangle_{\rm flux}$ in MeV^2, L_ν in 10^{51} erg s^{-1}.

flux parameters are measured at this radius because farther out Doppler effects of the original model would make it difficult to compare the results. Keeping in mind that we use very different numerical approaches and somewhat different input physics, the agreement in particular for $\nu_{\rm e}$ and $\bar\nu_{\rm e}$ is remarkably good. This agreement shows once more that our Monte Carlo approach likely captures at least the differential effects of the new microphysics in a satisfactory manner.

In Fig. 8 we compare our calculations for the Accretion-Phase Model II with those of the original simulation. The step-like curve again represents the mean energy of neutrinos in LTE for zero chemical potential. The smooth solid line is the mean energy $\langle\epsilon\rangle$ from our runs, the dotted (lower) line gives $\langle\epsilon\rangle_{\rm flux}$. The crosses are the corresponding results from the original runs. For the transport of ν_μ our inner boundary is $R_{\rm in} = 16$ km, while for $\nu_{\rm e}$ and $\bar\nu_{\rm e}$ we use $R_{\rm in} = 24$ km. For $\nu_{\rm e}$ and $\bar\nu_{\rm e}$ the charged-current processes (urca) keep these neutrinos in LTE up to larger radii than pair processes in the case of ν_μ. With our choice of $R_{\rm in}$ the neutrinos are in LTE within the innermost radial zones.

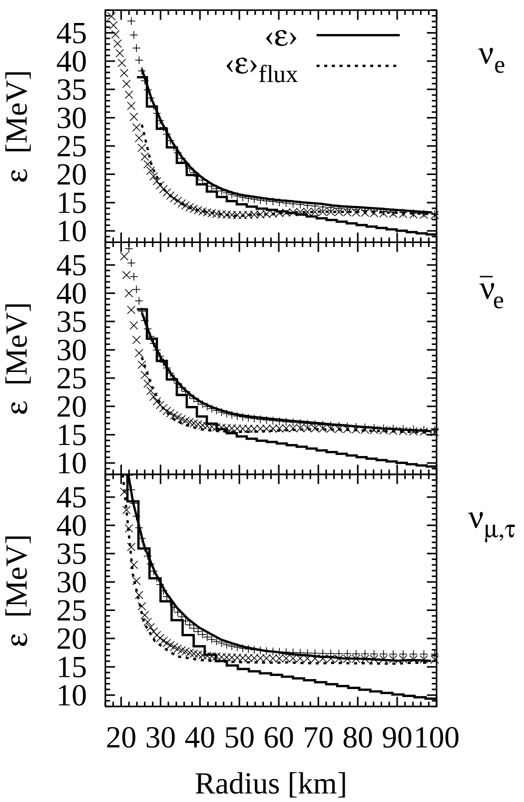

Fig. 8.— Comparison of the Accretion-Phase Model II calculations. Continuous lines show our Monte Carlo runs while crosses represent the original simulation by Rampp. The steps correspond to $\langle\epsilon\rangle = 3.15\,T$.

The results are similar to the Accretion-Phase Model I. The luminosities are not equipartitioned but instead follow roughly $L_{\nu_{\rm e}} \approx L_{\bar\nu_{\rm e}} \approx 2\,L_{\nu_\mu}$. The ratios of mean energies are $\langle\epsilon_{\nu_{\rm e}}\rangle : \langle\epsilon_{\bar\nu_{\rm e}}\rangle : \langle\epsilon_{\nu_\mu}\rangle = 0.82 : 1 : 1.09$ in the original run and $0.84 : 1 : 1.02$ in our run.

In summary, both accretion-phase models agree reasonably well in the $\langle\epsilon_{\nu_{\rm e}}\rangle : \langle\epsilon_{\bar\nu_{\rm e}}\rangle$ ratio for all runs. Moreover, using traditional input physics one finds something like $\langle\epsilon_{\bar\nu_{\rm e}}\rangle : \langle\epsilon_{\nu_\mu}\rangle = 1 : 1.20$. Depending on the implementation of the new input physics and depending on the model one finds results between $\langle\epsilon_{\bar\nu_{\rm e}}\rangle : \langle\epsilon_{\nu_\mu}\rangle = 1 : 1.02$ and $1 : 1.09$. The higher ratio in Rampp's simulation could be due to the inclusion of weak magnetism which tends to raise $\langle\epsilon_{\nu_\mu}\rangle$ more than $\langle\epsilon_{\bar\nu_{\rm e}}\rangle$.

In order to estimate the corresponding results for later stages of the proto-neutron star evolution we employ our steep power-law model. We vary the power q of the temperature profile within a reasonable range so that $q/p = 0.25$–0.35, with q and p defined in Eq. (3). $Y_{\rm e}$ is fixed by demanding roughly equal number fluxes for $\nu_{\rm e}$ and $\bar\nu_{\rm e}$ because a few seconds after bounce deleptonization should be essentially complete. The fluxes of these neutrinos depend very sensitively on $Y_{\rm e}$ so that this constraint is only reached to within about 30% without tuning $Y_{\rm e}$ to three decimal places. However, the mean energies are rather insensitive to the exact value of $Y_{\rm e}$. This is illustrated by the steep power-law model with $q = 2.5$ where we show results for $Y_{\rm e} = 0.15$ and 0.20. The number fluxes of $\nu_{\rm e}$ and $\bar\nu_{\rm e}$ differ by less than 30% for $Y_{\rm e} = 0.15$, but differ by a factor of 3 for $Y_{\rm e} = 0.2$. At the same time, the average spectral energies barely change.

The ratios of mean energies are not very different from those of the accretion-phase models. Of course, the absolute flux energies have no physical meaning because we adjusted the stellar profile in order to obtain realistic values. For the luminosities we find $L_{\nu_{\rm e}} < L_{\nu_\mu}$, different from the accretion phase. The steep power law implies that the radiating surfaces are similar for all flavors so that it is not surprising that the flavor with the largest energies also produces the largest luminosity.

We find that $\langle\epsilon_{\nu_\mu}\rangle$ always exceeds $\langle\epsilon_{\bar\nu_{\rm e}}\rangle$ by a small amount, the exact value depending on the stellar model. During the accretion phase the energies seem to be almost identical, later they may differ by up to 20%. We have not found a model where the energies differ by the large amounts which are sometimes assumed in the literature. At late times when $Y_{\rm e}$ is small the microphysics governing $\bar\nu_{\rm e}$ transport is closer to that for ν_μ than at early times. Therefore, one expects that at late times the behavior of $\bar\nu_{\rm e}$ is more similar to ν_μ than at early times. We do not see any argument for expecting an extreme hierarchy of energies at late times for self-consistent stellar models.

We never find exact equipartition of the flavor-dependent luminosities. Depending on the stellar profile the fluxes can mutually differ by up to a factor of 2 in either direction.

4.2. Previous Literature

There is a large recent body of literature quoted in our introduction where the effect of flavor oscillations on SN neutrino spectra and fluxes is studied. Many of these papers assumed that $\langle\epsilon_{\nu_\mu}\rangle$ is much larger than $\langle\epsilon_{\bar\nu_{\rm e}}\rangle$ and that the luminosities between all flavors were exactly equipartitioned. Our findings here are almost orthogonal to this perception. Where does it come from?

To the best of our knowledge, the microphysics employed for ν_μ transport is roughly the same in all published simulations. It includes iso-energetic scattering on nucleons, $\rm e^+e^-$ annihilation and $\nu_\mu \rm e^\pm$ scattering. Of course, the transport method and the numerical implementation of the neutrino processes differ in the codes of different groups. The new reactions and nucleon recoil lower $\langle\epsilon_{\nu_\mu}\rangle$ and modify the luminosities, but not by such a large amount as to explain a completely different paradigm. Therefore, we have inspected the previous literature and collect a representative sample of pertinent results in Table 6. Note that the simulations discussed below did not in all cases use the same stellar models and equations of state for the dense matter in the supernova core.

We begin with the simulations of the Livermore group who find robust explosions by virtue of the neutron-finger convection phenomenon. Neutrino transport is treated in the hydrodynamical models with a multigroup flux-limited diffusion scheme. Mayle, Wilson, & Schramm (1987) gave detailed results for their SN simulation of a $25\,M_\odot$ star. For half a second after bounce they obtained a somewhat oscillatory behavior of the neutrino luminosities. After the prompt peak of the electron neutrino luminosity, they got $L_{\nu_{\rm e}} \approx L_{\bar\nu_{\rm e}} \approx 2\,L_{\nu_\mu} \approx$ 50–130×10^{51} erg s^{-1}. After about one second the values stabilize. This calculation did not produce the "standard" hierarchy of energies. However, there is clearly a tendency that $\bar\nu_{\rm e}$ behave more similar to ν_μ at late times.

The most recent published Livermore simulation is a $20\,M_\odot$ star (Totani et al. 1998). It shows an astonishing degree of luminosity equipartition from the accretion phase througout the early Kelvin-Helmholtz cooling phase. About two seconds after bounce the ν_μ flux falls off more slowly than the other flavors. In Table 6 we show representative results for an early and a late time. The mean energies and their ratios are consistent with what we would have expected on the basis of our study.

With a different numerical code, Bruenn (1987) found for a $25\,M_\odot$ progenitor qualitatively different results for luminosities and energies. At about 0.5 s after bounce the luminosities and energies became stable at the values given in Table 6. This simulation is an example for an extreme hierarchy of mean energies.

In Burrows (1988) all luminosities are said to be equal. In addition it is stated that for the first 5 seconds $\langle\epsilon_{\nu_\mu}\rangle \approx 24$ MeV and the relation to the other flavors is $\langle\epsilon_{\nu_{\rm e}}\rangle : \langle\epsilon_{\bar\nu_{\rm e}}\rangle : \langle\epsilon_{\nu_\mu}\rangle = 0.9 : 1 : 1.8$. Detailed results are only given for $\bar\nu_{\rm e}$, so we are not able to add this reference to our table. The large variety of models investigated by Burrows (1988) and the detailed results for $\bar\nu_{\rm e}$ go beyond the scope of our brief description. In a later paper Myra & Burrows (1990) studied a $13\,M_\odot$ progenitor model and found the extreme hierarchy of energies shown in our table.

With the original version of our code Janka & Hillebrandt (1989b) performed their analyses for a $20\,M_\odot$ progenitor from a core-collapse calculation by Hillebrandt (1987). Of course, like our present study, these were Monte Carlo simulations on a

Table 6

Flavor dependent flux characteristics from the literature.

	tpb	$\langle\epsilon_{\nu_e}\rangle$	$\langle\epsilon_{\bar\nu_e}\rangle$	$\langle\epsilon_{\nu_\mu}\rangle$	$\frac{\langle\epsilon_\nu\rangle}{\langle\epsilon_{\bar\nu_e}\rangle}$	L_{ν_e}	$L_{\bar\nu_e}$	L_{ν_μ}
Mayle et al. (1987)	1.0	12	24	22	0.50 : 1 : 0.92	20	20	20
Totani et al. (1998)	0.3	12	15	19	0.80 : 1 : 1.26	20	20	20
	10	11	20	25	0.55 : 1 : 1.25	0.5	0.5	1
Bruenn (1987)	0.5	10	12	25	0.83 : 1 : 2.08	3	5	16
Myra & Burrows (1990)	0.13	11	13	24	0.85 : 1 : 1.85	30	30	16
Janka & Hillebrandt (1989b)	0.3	8	14	16	0.57 : 1 : 1.14	30	220	65
Suzuki (1990)	1	9.5	13	15	0.73 : 1 : 1.15	4	4	3
	20	8	10	9	0.80 : 1 : 0.90	0.3	0.3	0.07
Suzuki (1991)	1	9.5	13	15	0.73 : 1 : 1.15	3	3	3
	15	8	9	9.5	0.89 : 1 : 1.06	0.4	0.4	0.3
Suzuki (1993)	1	9	12	13	0.75 : 1 : 1.08	3	3	3
	15	7	8	8	0.88 : 1 : 1.00	0.3	0.3	0.3
Accretion-Phase Model I (original)	0.32	13	15	18	0.86 : 1 : 1.20	31	29	14
Accretion-Phase Model I (our run)	0.32	12	14	14	0.84 : 1 : 1.02	32	32	18
Accretion-Phase Model II (original)	0.15	13	16	17	0.82 : 1 : 1.09	66	68	32
Accretion-Phase Model II (our run)	0.15	13	15	16	0.84 : 1 : 1.02	74	74	28
The following lines show $\langle\epsilon\rangle_{\rm rms}$ instead of $\langle\epsilon\rangle$								
Mezzacappa et al. (2001)	0.5	16	19	24	0.84 : 1 : 1.26	25	25	8
Liebendörfer et al. (2001)	0.5	19	21	24	0.90 : 1 : 1.14	30	30	10

Note.—We give the time post bounce (tpb) in s, $\langle\epsilon\rangle$ in MeV, and L_ν in 10^{51} erg s^{-1}.

fixed background model, not self-consistent simulations. Taking into account the different microphysics the mean energies are consistent with our present work. The mean energies of ν_e were somewhat on the low side relative to $\bar{\nu}_e$ and the $\bar{\nu}_e$ luminosity was overestimated. Both can be understood by the fact that the stellar background contained an overly large abundance of neutrons, because the model resulted from a post-bounce calculation which only included electron neutrino transport.

Suzuki (1990) studied models with initial temperature and density profiles typical of proto-neutron stars at the beginning of the Kelvin-Helmholtz cooling phase about half a second after bounce. He used the relatively stiff nuclear equation of state developed by Hillebrandt & Wolff (1985). In our table we show the results of the model C12. From Suzuki (1991) we took the model labeled C20 which includes bremsstrahlung. The model C48 from Suzuki (1993) includes multiple-scattering suppression of bremsstrahlung. Suzuki's models are the only ones from the previous literature which go beyond the traditional microphysics for ν_μ transport. It is reassuring that his ratios of mean energies come closest to the ones we find.

Over the past few years, first results from Boltzmann solvers coupled with hydrodynamical simulations have become available, notably the unpublished ones that we used as our Accretion-Phase Models I and II. For convenience we include them in Table 6. Moreover, we include two simulations similar to the Accretion-Phase Model I, one by Mezzacappa et al. (2001) and the other by Liebendörfer et al. (2001). These latter papers show rms energies instead of mean energies. Recalling that the former tend to be about 45% larger than the latter these results are entirely consistent with our Accretion-Phase Models. Moreover, the ratios of $\langle\epsilon\rangle_{\rm rms}$ tend to exaggerate the spread between the flavor-dependent mean energies because of different amounts of spectral pinching, i.e. different effective degeneracy parameters. To illustrate this point we take the first two rows from Table 5 as an example. The ratio of mean energies for Fermi-Dirac spectra with temperatures $T_1 = 5.2$ and $T_2 = 3.5$ and degeneracy parameters $\eta_1 = 1.1$ and $\eta_2 = 3.4$ is $\langle\epsilon_1\rangle/\langle\epsilon_2\rangle = 1.19$, whereas the ratio of rms energies equals 1.30.

To summarize, the frequently assumed exact equipartition of the emitted energy among all flavors appears only in some simulations of the Livermore group. We note that the flavor-dependent luminosities tend to be quite sensitive to the detailed atmospheric structure and chemical composition. On the other hand, the often-assumed extreme hierarchy of mean energies was only found in the early simulations of Bruenn (1987) and of Myra & Burrows (1990), possibly a consequence of the neutron-star equation of state used in these calculations.

If we ignore results which appear to be "outliers", the picture emerging from Table 6 is quite consistent with our own findings. For the luminosities, typically $L_{\nu_e} \approx L_{\bar{\nu}_e}$ and a factor of 2–3 between this and L_{ν_μ} in either direction, depending on the evolutionary phase. For the mean energies we read typical ratios in the range of $\langle\epsilon_{\nu_e}\rangle : \langle\epsilon_{\bar{\nu}_e}\rangle : \langle\epsilon_{\nu_\mu}\rangle = 0.8\text{–}0.9 : 1 : 1.1\text{–}1.3$. The more recent simulations involving a Boltzmann solvers show a consistent behavior and will in future provide reliable information about neutrino fluxes and spectra.

5. DISCUSSION AND SUMMARY

We have studied the formation of neutrino spectra and fluxes in a SN core. Using a Monte Carlo code for neutrino transport, we varied the microscopic input physics as well as the underlying static proto-neutron star atmosphere. We used two background models from self-consistent hydrodynamical simulations, and several power-law models with varying power-law indices for the density and temperature and different values for the electron fraction Y_e, taken to be constant.

The ν_μ transport opacity is dominated by neutral-current scattering on nucleons. In addition, there are number-changing processes (nucleon bremsstrahlung, leptonic pair annihilation) and energy-changing processes (nucleon recoil, $\nu_\mu e^\pm$ scattering). The ν_μ spectra and fluxes are roughly accounted for if one includes one significant channel of pair production and one for energy exchange in addition to ν_μN scattering. For example, the traditional set of microphysics (isoenergetic ν_μN scattering, e^+e^- annihilation, and $\nu_\mu e^\pm$ scattering) yields comparable spectra and fluxes to a calculation where pairs are produced by nucleon bremsstrahlung and energy is exchanged by nucleon recoil. The overall result is quite robust against the detailed choice of microphysics.

However, in state-of-the-art simulations where one aims at a precision better than some 10–20% for the fluxes and spectral energies, one needs to include bremsstrahlung, leptonic pair annihilation, neutrino-electron scattering, and energy transfer in neutrino-nucleon collisions. Interestingly, the traditional e^+e^- annihilation process is always much less important than $\nu_e\bar{\nu}_e$ annihilation, a point that we previously raised with our collaborators (Buras et al. 2002). None of the reactions studied here can be neglected except perhaps the traditional e^+e^- annihilation process and $\nu_\mu\nu_e$ and $\nu_\mu\bar{\nu}_e$ scattering.

The existing treatments of the nuclear-physics aspects of the $\mathrm{NN} \to \mathrm{NN}\nu\bar{\nu}$ bremsstrahlung process are rather schematic. We find, however, that the ν_μ fluxes and spectra do not depend sensitively on the exact strength of the bremsstrahlung rate. Therefore, while a more adequate treatment of bremsstrahlung remains desirable, the final results are unlikely to be much affected.

Including all processes works in the direction of making the fluxes and spectra of ν_μ more similar to those of $\bar{\nu}_e$ compared to a calculation with the traditional set of input physics. During the accretion phase the neutron-star atmosphere is relatively expanded, i.e. the density and temperature gradients are relatively shallow. Our investigation suggests that during this phase $\langle\epsilon_{\nu_\mu}\rangle$ is only slightly larger than $\langle\epsilon_{\bar{\nu}_e}\rangle$, perhaps by a few percent or 10% at most. This result agrees with the first hydrodynamical simulation including all of the relevant microphysics except $\nu_e\bar{\nu}_e$ annihilation (Accretion-Phase Model II) provided to us by M. Rampp. For the luminosities of the different neutrino species one finds $L_{\bar{\nu}_e} \sim L_{\nu_e} \sim 2\,L_{\nu_\mu}$. The smallness of L_{ν_μ} is not surprising because the effective radiating surface is much smaller than for $\bar{\nu}_e$.

During the Kelvin-Helmholtz cooling phase the neutron-star atmosphere will be more compact, the density and temperature gradients will be steeper. Therefore, the radiating surfaces for all species will become more similar. In this situation L_{ν_μ} may well become larger than $L_{\bar{\nu}_e}$. However, the relative luminosities depend sensitively on the electron concentration. Therefore, without a self-consistent hydrostatic late-time model it is difficult to claim this luminosity cross-over with confidence.

The ratio of the spectral energies is most sensitive to the temperature gradient relative to the density gradient. In our power-law models we used $\rho \propto r^{-p}$ and $T \propto r^{-q}$. Varying q/p between 0.25 and 0.35 we find that $\langle\epsilon_{\bar{\nu}_e}\rangle : \langle\epsilon_{\nu_\mu}\rangle$ varies between $1 : 1.10$ and $1 : 1.22$. Noting that the upper range for q/p seems unrealistically large we conclude that even at late times the spectral differences should be small; 20% sounds like a safe upper limit. We are looking forward to this prediction being checked in a full-scale self-consistent neutron-star evolution model with a Boltzmann solver.

The statements in the previous literature fall into two classes. One group of workers, using the traditional set of microphysics, found spectral differences between $\bar{\nu}_e$ and ν_μ on the 25% level, a range which largely agrees with our findings in view of the different microphysics. Other papers claim ratios as large as $\langle\epsilon_{\bar{\nu}_e}\rangle : \langle\epsilon_{\nu_\mu}\rangle = 1 : 1.8$ or even exceeding $1 : 2$. We have no explanation for these latter results. At least within the framework of our simple power-law models we do not understand which parameter could be reasonably adjusted to reach such extreme spectral differences.

In a high-statistics neutrino observation of a future galactic SN one may well be able to discover signatures for flavor oscillations. However, when studying these questions one has to allow for the possibility of very small spectral differences, and conversely, for the possibility of large flux differences. This situation is orthogonal to what often has been assumed in papers studying possible oscillation signatures.

We have always assumed that ν_μ and $\bar{\nu}_\mu$ behave identically. However, weak-magnetism effects render the $\nu_\mu\mathrm{N}$ and $\bar{\nu}_\mu\mathrm{N}$ scattering cross sections somewhat different (see, e.g., Horowitz 2002). To study the resulting differences of the ν_μ and $\bar{\nu}_\mu$ fluxes and spectra requires a modified setup of our Monte Carlo code because ν_μ and $\bar{\nu}_\mu$ have to be transported simultaneously. The different transport coefficients will cause a ν_μ chemical potential to build up. While we expect the differences of fluxes and spectra to be small, we intend to investigate this issue quantitatively in the near future.

ACKNOWLEDGMENTS

We thank the Institute for Nuclear Theory (University of Washington, Seattle) for its hospitality during a visit when this work was begun. In Munich, this work was partly supported by the Deutsche Forschungsgemeinschaft under grant No. SFB 375 and by the ESF network Neutrino Astrophysics. We thank Bronson Messer and Markus Rampp for providing unpublished stellar profiles from self-consistent collapse simulations.

A. MONTE CARLO CODE

Our Monte Carlo code is based on that developed by Janka (1987) where a detailed description of the numerical aspects can be found. The code was first applied to calculations of neutrino transport in supernovae by Janka & Hillebrandt (1989a,b) and Janka (1991). It uses Monte Carlo methods to follow the individual destinies of sample neutrinos (particle "packages" with suitably attributed weights to represent a number of real neutrinos) on their way through the star from the moment of creation or inflow to their absorption or escape through the inner or outer boundaries. The considered stellar background is assumed to be spherically symmetric and static, and the sample neutrinos are characterized by their weight factors and by continuous values of energy, radial position and direction of motion, represented by the cosine of the angle relative to the radial direction. The rates of neutrino interactions with particles of the stellar medium can be evaluated by taking into account Fermion blocking effects according to the local phase-space distributions of neutrinos (Janka & Hillebrandt 1989b).

As background stellar models we use the ones described in Sec. 2.2. They are defined by radial profiles of the density ρ, temperature T, and electron fraction $Y_{\rm e}$, i.e. the number of electrons per baryon. The calculations span the range between some inner radius $R_{\rm in}$ and outer radius $R_{\rm out}$. These bound the computational domain which is divided into 30 equally spaced radial zones. In each zone ρ, T, and $Y_{\rm e}$ are taken to be constant. $R_{\rm in}$ is chosen at such high density and temperature that the neutrinos are in LTE in at least the first radial zone. $R_{\rm out}$ is placed in a region where the neutrinos essentially stream freely. At $R_{\rm in}$ neutrinos are injected isotropically according to LTE. While a small net flux across the inner boundary develops, the neutrinos emerging from the star are generated almost exclusively within our computational domain. If $R_{\rm in}$ is chosen so deep that the neutrinos are in LTE, the assumed boundary condition for the flux will therefore not affect the results.

The stellar medium is assumed to be in thermodynamic equilibrium with nuclei being completely disintegrated into free nucleons. Based on ρ, T, and $Y_{\rm e}$ we calculate all the required thermodynamical quantities, notably the number densities, chemical potentials, and temperatures of protons, neutrons, electrons, positrons, and the relevant neutrinos. The chemical potentials for ν_μ and ν_τ are taken to be zero. Next we compute the interaction rates in each radial zone for all included processes. In the simulations discussed in the present work, fermion phase-space blocking is calculated from the neutrino equilibrium distributions instead of the computed phase-space distributions. This simplification saves a lot of CPU time because otherwise the rates have to be reevaluated whenever the distribution of neutrinos has changed after a transport time step. The approximation is justified because phase-space blocking is most important in regions where neutrinos frequently interact and thus are close to LTE.

At the start of a Monte Carlo run, 800,000 test neutrinos are randomly distributed in the model according to the local equilibrium distributions. Each test neutrino represents a certain number of real neutrinos. In this initial setup the number of real neutrinos is determined by LTE. Then transport is started. The time step is fixed at $\Delta t = 10^{-7}s$; recall that the interaction rates do not change. At the beginning of each step neutrino creation takes place. The number of test particles that can be created is given by the number of neutrinos that were lost through the inner and outer boundaries plus those absorbed by the medium. Based on Δt, the production rates, and the fact that the inner boundary radiates neutrinos, we calculate the number of neutrinos that are produced in one time step and distribute them among the available test neutrinos by attributing suitable weight factors. The sample particles are created within the medium or injected at the inner boundary in appropriate proportions.

During a time step the path of each test particle through the stellar atmosphere is followed by Monte Carlo sampling. With random numbers we decide whether it flies freely or interacts. If it interacts it can scatter or it can be absorbed; in this case we turn to the next particle. For scattering we determine the new momentum and position and continue with the process until the time step is used up. Particles leaving through the lower or upper boundaries are eliminated from the transport.

After a certain number of time steps (typically around 15,000) the neutrino distribution reaches a stationary state and further changes occur only due to statistical fluctuations. At that stage we start averaging the output quantities over the next 500 time steps.

B. NEUTRINO PROCESSES

B.1. Neutrino-Nucleon Scattering

The rates for the ν_μN reactions are calculated following Raffelt (2001). For a neutrino with initial energy ϵ_1 and final energy ϵ_2, the differential cross section is given by

$$\frac{d\sigma}{d\epsilon_2\, d\cos\theta} = \frac{C_A^2(3-\cos\theta)}{2\pi}\, G_F^2\, \epsilon_2^2\, \frac{S(\omega,k)}{2\pi} \qquad \text{(B1)}$$

with $\omega = \epsilon_1 - \epsilon_2$, k the modulus of the momentum transfer to the medium, and θ the scattering angle. We do not distinguish between protons and neutrons. Since for nonrelativistic nucleons the scattering cross section is proportional to $C_V^2 + 3C_A^2$, the vector current ($C_V = -\frac{1}{2}$ for neutrons and $\frac{1}{2} - 2\sin^2\Theta_{\rm W}$ for protons) is small compared to the axial component, where we use $|C_A| = 1.26/2$. Neglecting the vector part simplifies the calculations significantly and certainly has a smaller effect on the scattering rates than other uncertainties, for example the in-medium value of the coupling constants themselves.

In all of our runs without recoil the structure function is given by

$$S_{\rm no-recoil}(\omega,k) = 2\pi\delta(\omega)\,. \qquad \text{(B2)}$$

This corresponds to infinitely heavy nucleons and represents the traditional approximation in all previous simulations. For the more realistic case of recoiling nucleons the structure function becomes

$$S_{\rm recoil}(\omega,k) = \sqrt{\frac{\pi}{\omega_k T}}\, \exp\left(-\frac{\omega-\omega_k}{4T\omega_k}\right) \qquad \text{(B3)}$$

with $\omega_k = k^2/2m$.

Multiplying Eq. (B1) with the density of nucleons, ignoring phase space blocking of the essentially nondegenerate nucleons, yields the differential rates that can then be integrated for obtaining the required energy and angular differential rates. In the case of recoil the numerical integrations are rather tricky because Eq. (B1) is strongly forward peaked. In our code we employ the "rejection method" for obtaining the integrated rates (Press 1992).

B.2. Bremsstrahlung

We also follow Raffelt (2001). The mfp for the absorption of a ν_μ by inverse bremsstrahlung $\mathrm{NN}\nu_\mu\bar\nu_\mu \to \mathrm{NN}$ is given by

$$\begin{aligned}\lambda_{\rm brems}^{-1} &= \frac{C_A^2 G_F^2}{2}\, n_B\, \frac{1}{2\epsilon} \\ &\times \int \frac{d^3\bar k}{2\bar\epsilon\,(2\pi)^3}\, f(\bar\epsilon)\, 24\,\epsilon\,\bar\epsilon\, S(\epsilon+\bar\epsilon)\,. \end{aligned} \qquad \text{(B4)}$$

The over-barred quantities belong to the $\bar\nu_\mu$ that is absorbed together with the primary ν_μ. The occupation numbers are taken to follow an equilibrium distribution with zero chemical potential, and $\mid C_A \mid = 1.26/2$ as in the scattering case.

B.3. Pair Annihilation

We now turn to $\mathrm{e^+e^-} \to \nu_\mu\bar\nu_\mu$ and $\nu_{\rm e}\bar\nu_{\rm e} \to \nu_\mu\bar\nu_\mu$. The matrix elements for both processes are identical up to coupling constants while the phase-space integrations only differ by the chemical potentials.

After summing over all spins and neglecting the rest masses, the squared matrix element is

$$\begin{aligned}\sum_{\rm spins} |\mathcal{M}|^2 &= 8\, G_F^2 \Big[(C_V+C_A)^2 u^2 \\ &\quad + (C_V-C_A)^2 t^2\Big] \end{aligned} \qquad \text{(B5)}$$

with the Mandelstam variables $t = -2k_1\cdot k_3$ and $u = -2k_1\cdot k_4$. The momenta are assigned to the particles as indicated in Fig. 9. The weak interaction constants for e^+e^- annihilation are

$$C_V = -\frac{1}{2} + 2\sin^2\Theta_W\ , \quad C_A = -\frac{1}{2} \tag{B6}$$

while for $\nu_e\bar{\nu}_e$ annihilation they are

$$C_A = C_V = \frac{1}{2}\ . \tag{B7}$$

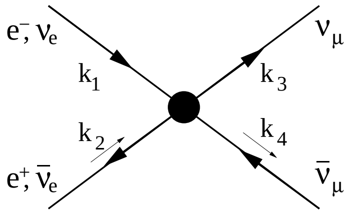

Fig. 9.— Pair annihilation processes producing $\nu_\mu\bar{\nu}_\mu$ pairs.

For the interaction rates we have to perform the phase-space integrations, using blocking factors for the final states and occupation numbers for initial-state particles (Hannestad & Madsen 1995, Yueh & Buchler 1976). Three integrations remain that can not be carried out analytically.

Mu- and tau-leptons are almost absent in protoneutron star atmospheres so that the chemical potentials of the corresponding neutrinos can be set to zero. For the e^+e^- reactions the local value of $\mu_{e^-} = -\mu_{e^+} \equiv \mu_e$ can be obtained from ρ, T, and Y_e by inverting

$$\frac{n_{e^-}(\mu_e) - n_{e^+}(\mu_e)}{n_{\rm baryons}} = Y_e\ , \tag{B8}$$

where $n_{e^-}(\mu_e)$ and $n_{e^+}(\mu_e)$ are Fermi integrals. For ν_e and $\bar{\nu}_e$ the chemical potential is obtained by the relation

$$\mu_{\nu_e} = -\mu_{\bar{\nu}_e} = \mu_e + \mu_p - \mu_n \tag{B9}$$

with the chemical potentials μ_p and μ_n of protons and neutrons, respectively.

For $\nu_e\bar{\nu}_e$ annihilation we make use of the fact that the energy sphere of ν_μ lies always deeper inside the star than the ν_e and $\bar{\nu}_e$ spheres (see Fig. 3). Thus ν_e and $\bar{\nu}_e$ are in LTE and are part of the medium as far as the transport of ν_μ is concerned. This approximation breaks down at larger radii where this process is unimportant anyway.

For our numerical implementation we normally use Fermi-Dirac statistics, but in order to reduce computation time one of the remaining three phase-space integrations is approximated by the analytic expressions given in Takahashi, El Eid, & Hillebrandt (1978). This also requires simplifying the blocking factors. With $\mu_e = -\mu_{e^+} \geq 0$ we can approximate the positron occupation number by a Maxwell-Boltzmann distribution. For $\mu_e/T \gtrsim 2$ this holds to very good accuracy. The greatest deviation is at $\mu_e/T = 0$ and yields blocking factors too low by about 10%. However, e^- and ν_e are always degenerate in the relevant regions.

B.4. Scattering on Electrons and Electron Neutrinos

The matrix elements for these reactions are just the crossed versions of the leptonic pair processes,

$$\sum_{\rm spins} |\mathcal{M}|^2 \;=\; 8\, G_F^2 \Big[(C_V + C_A)^2 s^2 + (C_V - C_A)^2 u^2\Big] \tag{B10}$$

with the same weak interaction coefficients of Eqs. (B6) or (B7) for scattering on e^- or on ν_e, respectively. For $s = 2k_1\cdot k_2$ and $u = -2k_1\cdot k_4$ the momenta are assigned to the particles according to Fig. 10. Crossing the matrix element Eq. (B10) again by interchanging $u \leftrightarrow t$, we obtain scattering on e^+ or $\bar{\nu}_e$. This is also true for scattering of $\bar{\nu}_\mu$ on e^- or ν_e; scattering of $\bar{\nu}_\mu$ on e^+ or $\bar{\nu}_e$ brings us back to Eq. (B10). For calculating the rates in our code we apply the same approximations as in the previous section.

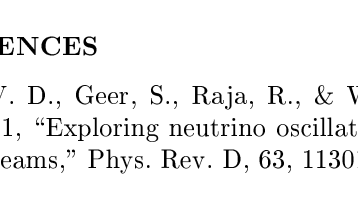

Fig. 10.— Leptonic scattering processes.

REFERENCES

Barger, V. D., Geer, S., Raja, R., & Whisnant, K. 2001, "Exploring neutrino oscillations with superbeams," Phys. Rev. D, 63, 113011

Barger, V., Marfatia, D., & Wood, B. P. 2001, "Inverting a supernova: Neutrino mixing, temperatures and binding energies," hep-ph/0112125

Bruenn, S. W. 1987, "Neutrinos from SN1987A and current status of stellar-core collapse," Phys. Rev. Lett. 59, 938

Buccella, F., Esposito, S., Gualdi, C., & Miele, G. 1997, "Supernova neutrino energy spectra and the MSW effect," Z. Phys. C, 73, 633

Buras, R., Janka, H.-T., Keil, M. Th., Raffelt, G. G., & Rampp, M. 2002, "Electron neutrino pair annihilation: A new source for muon and tau neutrinos," submitted to Ap.J. (astro-ph/0205006)

Burrows, A. 1988, "Supernova neutrinos," Astrophys. J., 334, 891

Burrows, A. & Sawyer, R. F. 1998, "Effects of correlations on neutrino opacities in nuclear matter," Phys. Rev. C, 58, 554

Burrows, A. & Sawyer, R. F. 1999, "Many-body corrections to charged-current neutrino absorption rates in nuclear matter," Phys. Rev. C, 59, 510

Burrows, A., Young, T., Pinto, Ph., Eastman, R. & Thompson, T. A. 2000, "Supernova neutrinos and a new algorithm for neutrino transport and some applications," Astrophys. J., 539, 865

Carter, G. W. & Prakash, M. 2002, "The quenching of the axial coupling in nuclear and neutron-star matter," Phys. Lett. B, 525, 249

Cervera, A., Donini, A., Gavela, M. B., Gomez Cadenas, J. J., Hernandez, P., Mena, O., & Rigolin, S. 2000, "Golden measurements at a neutrino factory," Nucl. Phys. B, 579, 17 [Erratum ibid. 593, 731 (2000)]

Chiu, S. H. & Kuo, T. K. 2000, "Effects of neutrino temperatures and mass hierarchies on the detection of supernova neutrinos," Phys. Rev. D, 61, 073015

Dighe, A. S. & Smirnov, A. Y. 2000, "Identifying the neutrino mass spectrum from the neutrino burst from a supernova," Phys. Rev. D, 62, 033007

Dutta, G., Indumathi, D., Murthy, M. V., & Rajasekaran, G. 2000, "Neutrinos from stellar collapse: Comparison of the effects of three and four flavor mixings," Phys. Rev. D, 62, 093014

Freund, M., Huber, P., & Lindner, M. 2001, "Systematic exploration of the neutrino factory parameter space including errors and correlations," Nucl. Phys. B, 615, 331

Fryer, C. L. 1999, "Mass limits for black hole formation," Ap. J., 522, 413

Fryer, C. L. & Warren, M. S. 2002, "Modeling core-collapse supernovae in 3-dimensions," Ap. J. Lett., in press, astro-ph/0206017

Fuller, G. M., Haxton, W. C., & McLaughlin, G. C. 1999, "Prospects for detecting supernova neutrino flavor oscillations," Phys. Rev. D, 59, 085005

Fuller, G. M., Mayle, R., Meyer, B. S., & Wilson, J. R. 1992, "Can a closure mass neutrino help solve the supernova shock reheating problem?," Ap. J., 389, 517

Giovanoni, P. M., Ellison, D. C., & Bruenn, S. W. 1989, "Neutrino transport during the core bounce phase of a type II supernova explosion," Ap. J., 342, 416

Hannestad, S. & Madsen, J. 1995, "Neutrino decoupling in the early universe," Phys. Rev. D, 52, 1764

Hannestad, S. & Raffelt, G. 1998, "Supernova neutrino opacity from nucleon nucleon bremsstrahlung and related processes," Ap. J., 507, 339

Hillebrandt, W. 1987, "Stellar collapse and supernova explosions," in: High Energy Phenomena around Collapsed Stars," Procs. NATO ASI, 2–13 Sept. 1985, Cargèse, Corsica, France, edited by D. Pacini (Reidel, Dordrecht), p. 73

Hillebrandt, W. & Wolff, R. G. 1985, "Models of type II supernova explosions," in: Nucleosynthesis: Challenges and New Developments, edited by W.D. Arnett and J.W. Truran (University of Chicago Press, Chicago), p. 131

Horowitz, C. J. 2002, "Weak magnetism for antineutrinos in supernovae," Phys. Rev. D, 65, 043001

Janka, H.-T. 1987, “Monte-Carlo-Verfahren für den Neutrinotransport in Supernovae,” (Diploma Thesis, Technical University Munich)

Janka, H.-T. 1991, “Neutrino transport in type-II supernovae and protoneutron stars by Monte Carlo Methods,” (Ph.D. Thesis, Technical University Munich), MPA-Report 587

Janka, H.-T. 1993, “Neutrinos from type-II supernovae and the neutrino-driven supernova mechanism,” in: Proc. Vulcano Workshop 1992 Frontier Objects in Astrophysics and Particle Physics, 18–23 May 1992, Vulcano, Italy, edited by F. Giovannelli and G. Mannocchi (Società Italiana di Fisica, Bologna), p. 345

Janka, H.-T. & Hillebrandt, W. 1989a, “Neutrino emission from type II supernovae—an analysis of the spectra,” Astron. Astrophys., 224, 49

Janka, H.-T. & Hillebrandt, W. 1989b, “Monte Carlo simulations of neutrino transport in type II supernovae,” Astron. Astrophys. Suppl. Ser., 78, 375

Janka, H.-T., Keil, W., Raffelt, G., & Seckel, D. 1996, “Nucleon spin fluctuations and the supernova emission of neutrinos and axions,” Phys. Rev. Lett., 76, 2621

Jegerlehner, B., Neubig, F., & Raffelt, G. 1996 “Neutrino oscillations and the supernova 1987A Signal,” Phys. Rev. D, 54, 1194

Kachelriess, M., Strumia, A., Tomàs, R., & Valle, J. W. 2002, “SN1987A and the status of oscillation solutions to the solar neutrino problem,” arXiv:hep-ph/0108100

Liebendörfer, M., Mezzacappa, A., Thielemann, F.-K., Messer, O. E. B., Hix, W. R., & Bruenn, W. 2001, “Probing the gravitational well: No supernova explosion in spherical symmetry with general relativistic Boltzmann neutrino transport,” Phys. Rev. D, 63, 103004

Lunardini, C. & Smirnov, A. Y. 2001a, “Neutrinos from SN1987A, Earth matter effects and the LMA solution of the solar neutrino problem,” Phys. Rev. D, 63, 073009

Lunardini, C. & Smirnov, A. Y. 2001b, “Supernova neutrinos: Earth matter effects and neutrino mass spectrum,” Nucl. Phys. B, 616, 307

Mayle, R., Wilson, J. R., & Schramm, D. N. 1987, “Neutrinos from gravitational collapse,” Ap. J., 318, 288

Mezzacappa, A., Liebendörfer, M., Messer, O. E., Hix, W. R., Thielemann, F.-K., & Bruenn, S. W. 2001, “Simulation of the spherically symmetric stellar core collapse, bounce, postbounce evolution of a a star of 13 solar masses with Boltzmann neutrino transport, and its implications for the supernova mechanism,” Phys. Rev. Lett., 86, 1935

Minakata, H. & Nunokawa, H. 2001, “Inverted hierarchy of neutrino masses disfavored by supernova 1987A,” Phys. Lett. B, 504, 301

Minakata, H., Nunokawa, H., Tomàs, R., & Valle, J. W. F. 2001, “Probing supernova physics with neutrino oscillations,” hep-ph/0112160

Myra, E. S. & Burrows, A. 1990, “Neutrinos from type II supernovae: The first 100 milliseconds,” Ap. J., 364, 222

Myra, E. S., Lattimer, J. M., & Yahil, A. 1988, “Neutrino emission from cooling neutron stars,” in: Supernova 1987A in the Large Magellanic Cloud, Proc. Fourth George Mason Astrophysics Workshop, 12–14 Oct. 1987, Fairfax, Virginia, USA, edited by M. Kafatos and A. Michalitsianos (Cambridge University Press, Cambridge, England) p. 213

Press, W. H., Teukolsky, S. A., Vetterling, W. T. & Flannery, B. P. 1992, “Numerical Recipes in Fortran 77,” Second Edition, Vol. 1, (Cambridge University Press)

Qian, Y. Z., Fuller, G. M., Mathews, G. J., Mayle, R., Wilson, J. R., & Woosley, S. E. 1993, “A connection between flavor mixing of cosmologically significant neutrinos and heavy element nucleosynthesis in supernovae,” Phys. Rev. Lett., 71, 1965

Raffelt, G. G. 2001, “Mu- and tau-neutrino spectra formation in supernovae,” Ap. J., 561, 890

Rampp, M. & Janka, H.-T. 2000, “Spherically symmetric simulation with Boltzmann neutrino transport of core collapse and post-bounce evolution of a 15 solar mass star,” Ap. J., 539, L33

Rampp, M. & Janka, H.-T. 2002, "Radiation hydrodynamics with neutrinos: Variable Eddington factor method for core-collapse supernova simulations," submitted to Astron. Astrophys. (astro-ph/0203101)

Rampp, M., Buras, R., Janka, H.-T., Raffelt, G. 2002, "Core-collapse supernova simulations: Variations of the input physics," in: Procs. 11th Workshop on "Nuclear Astrophysics," Ringberg Castle, Tegernsee, Germany, Feb. 11–16, 2002, MPA-Report P13 (Max-Planck-Institut für Astrophysik, Garching), p. 119 (astro-ph/0203493)

Shapiro, S.L. & Teukolsky, S.A. 1983, "Black holes, white dwarfs and neutron stars: The physics of compact objects" (John Wiley & Sons, New York)

Smirnov, A. Y., Spergel, D. N., & Bahcall, J. N. 1994, "Is Large Lepton Mixing Excluded?," Phys. Rev. D, 49, 1389

Suzuki, H. 1990, "Neutrino burst from supernova explosion and proto neutron star cooling," (Ph.D. Thesis, University of Tokyo)

Suzuki, H. 1991, "Neutrino emission from protoneutron star with modified Urca and nucleon bremsstrahlung processes," Num. Astrophys. Japan, 2, 267

Suzuki, H. 1993, "Supernova neutrinos—Multigroup simulations of neutrinos from protoneutron star," in: Proc. International Symposium on Neutrino Astrophysics: Frontiers of Neutrino Astrophysics, 19–22 Oct. 1992, Takayama, Japan, edited by Y. Suzuki and K. Nakamura (Universal Academy Press, Tokyo)

Takahashi, K. & Sato, K. 2002, "Earth effects on supernova neutrinos and their implications for neutrino parameters," arXiv:hep-ph/0110105.

Takahashi, K., El Eid, M. F. E., & Hillebrandt, W. 1978, "Beta transition rates in hot and dense matter," Astron. Astrophys., 67, 185

Thompson, T. A., Burrows, A., & Horvath, J. E. 2000, "Mu and tau neutrino thermalization and production in supernovae: Processes and timescales," Phys. Rev. C, 62, 035802

Totani, T., Sato, K., Dalhed, H. E., & Wilson, J. R. 1998, "Future detection of supernova neutrino burst and explosion mechanism," Ap. J., 496, 216

Wilson, J. R. & Mayle, R. W. 1993, "Report on the progress of supernova research by the Livermore group," Phys. Rept., 227, 97

Yueh, W. R. & Buchler, J. R. 1976, "Scattering functions for neutrino transport," Astrophys. Space Sci., 39, 429.

This 2-column preprint was prepared with the AAS LaTeX macros v5.0.